

Equation-free patch scheme for efficient computational homogenisation via self-adjoint coupling

J. E. Bunder ^{*} I. G. Kevrekidis [†] A. J. Roberts [‡]

July 15, 2020

Abstract

Equation-free macroscale modelling is a systematic and rigorous computational methodology for efficiently predicting the dynamics of a microscale system at a desired macroscale system level. In this scheme, the given microscale model is computed in small patches spread across the space-time domain, with patch coupling conditions bridging the unsimulated space. For accurate simulations, care must be taken in designing the patch coupling conditions. Here we construct novel coupling conditions which preserve translational invariance, rotational invariance, and self-adjoint symmetry, thus guaranteeing that conservation laws associated with these symmetries are preserved in the macroscale simulation. Spectral and algebraic analyses of the proposed scheme in both one and two dimensions reveal mechanisms for further improving the accuracy of the simulations. Consistency of the patch scheme's

^{*}School of Mathematical Sciences, University of Adelaide, South Australia 5005, Australia. <http://orcid.org/0000-0001-5355-2288>, <mailto:judith.bunder@adelaide.edu.au>

[†]Departments of Chemical and Biomolecular Engineering and Applied Mathematics and Statistics, Johns Hopkins University, Baltimore, Maryland, USA. <http://orcid.org/0000-0002-5313-5887>

[‡]School of Mathematical Sciences, University of Adelaide, South Australia. <mailto:anthony.roberts@adelaide.edu.au>, <http://orcid.org/0000-0001-8930-1552>

macroscale dynamics with the original microscale model is proved. This new self-adjoint patch scheme provides an efficient, flexible, and accurate computational homogenisation in a wide range of multiscale scenarios of interest to scientists and engineers.

Contents

1	Introduction	2
2	Self-adjoint preserving patch scheme for 1D	8
2.1	Self-adjoint patch coupling for 1D	11
2.2	Spectral coupling of patches	15
2.3	Lagrangian spatial coupling of patches	18
2.3.1	Accuracy of Lagrangian patch coupling	21
2.4	An ensemble removes periodicity limitation	23
3	The patch scheme is consistent to high-order	28
3.1	An ensemble has the correct homogenisation	30
3.2	High-order consistency of the patch scheme	32
4	Self-adjoint preserving patch scheme for 2D	37
4.1	Self-adjoint coupling for 2D	38
4.2	An ensemble of phase-shifts appears accurate	42
4.3	This 2D patch scheme is consistent to high-order	46
5	Conclusion	51
A	Macroscale homogenise of 1D diffusion	58

1 Introduction

In many complex systems the macroscale dynamics are determined from the coherent behaviour of microscopic agents, such as electrons, molecules, or individuals in a population. Some complex systems have macroscale

models which adequately describe the large-scale dynamics (e.g., diffusion through a homogenous material), but for many others there are no known algebraic closures for a macroscale model and so any accurate description of the system is reliant on resolving microscale structures and interactions which are on a significantly smaller scale than the macroscale of interest. Furthermore, often a microscale model provides the most accurate description of a system, but its full evaluation is prohibitively expensive for large-scale computations. Although an approximate macroscale model may be derivable via various multiscale methods, such derivations are often reliant on restrictive assumptions or ad hoc methods which may not be suitable for all systems. In a recent review for NASA, Liu et al. (2018) discussed the accuracy and adaptability of available multiscale methods and concluded that there is a “Lack of useful automatic methods for linking models and passing information between scales”. Our equation-free computational schemes fill this lack by using a given microscale model directly, with no simplification or transformation, and invoking generically crafted coupling conditions to ensure macroscale accuracy.

Equation-free macroscale modelling avoids the derivation of a macroscale model and seeks to overcome computational limitations by computing the given microscale model only within a small fraction of the space-time domain (Kevrekidis, Gear, and Hummer 2004; Samaey, Kevrekidis, and Roose 2005; Samaey, Roose, and Kevrekidis 2006). As an example, Figure 1 shows an equation-free simulation of two dimensional diffusion, with microscale heterogeneity in the diffusivities. In this simulation the microscale details of the system are not computed in the space between the patches. Nonetheless the patch scheme effectively predicts the macroscale dynamics—it is a form of computational homogenisation via a sparse simulation. In a ‘Roadmap’ prepared for the US Dept of Energy by Dolbow, Khaleel, and Mitchell (2004), the scheme proposed here is a Multiresolution, Hybrid, Closure Method.

To suitably classify our equation-free scheme we distinguish the following two terms:

- *numerical homogenisation* means some numerical computations and analysis of the microscale system that somehow forms a function that

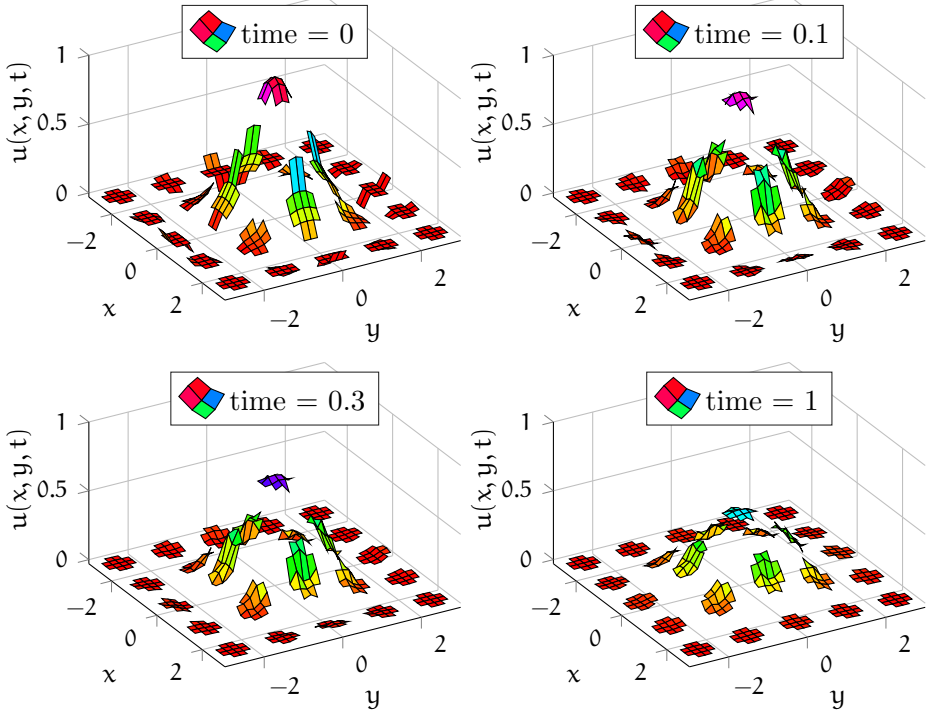
serves as a closure for chosen macroscale variables (Engquist and Souganidis 2008; Saeb, Steinmann, and Javili 2016);

- *computational homogenisation* means an on-the-fly purely computational scheme, applied to the multiscale system, that in itself provides an effective closure which reasonably predicts the macroscale dynamics with a computational cost that is essentially independent of the scale separation between micro- and macro-scales (Kevrekidis and Samaey 2009; Gear, Li, and Kevrekidis 2003).

The patch scheme developed herein is an example of computational homogenisation.

Much of the initial development of equation-free modelling was concerned with simulations which reduce the size of the temporal domain and maintain the original spatial domain (Kevrekidis, Gear, and Hummer 2004; Kevrekidis and Samaey 2009; Samaey, Kevrekidis, and Roose 2005; Xiu and Kevrekidis 2005; Samaey, Roose, and Kevrekidis 2006). In this case the numerical solution is constructed from a large number of microscale simulations over short ‘bursts’ of time, with these bursts separated by some macroscale time step (significantly larger than the burst length) and a projective integrator providing the link between successive bursts. In contrast, Figure 1 shows a numerical solution for which the spatial domain is reduced to a number of non-overlapping patches, but without projective integration in time implemented. In this case, the dynamics which extends across the full spatial domain is captured by patch coupling conditions which interpolate between patches across the unsimulated space. A full implementation of equation-free modelling combines both projective integration and spatially coupled patches; however, here we focus just on patches in space (often referred to as the gap-tooth method (Gear, Li, and Kevrekidis 2003)) because we are concerned with preserving spatial symmetries of the original microscale model. In particular, we preserve translational invariance, rotational invariance and self-adjoint symmetry by deriving new patch coupling conditions. Roberts (2010) also constructed self-adjoint coupling conditions, but for overlapping patches, and only in the case of limited coupling. Sections 2 and 4 describe our new self-adjoint patch coupling scheme for 1D and 2D space, respectively.

Figure 1: four times of a simulation of heterogeneous diffusion (1) on small patches in 2D xy -space coupled by spectral interpolation (Section 2.2). Here the 25 patches are relatively large for visibility (size ratio $r = 0.4$). The heterogeneous, log-normal, diffusivities cause non-trivial sub-patch structures to emerge that are computationally homogenised by our patch scheme.



Patch coupling conditions are a crucial component in accurate patch simulations, and for systems with microscale heterogeneity particular care is required. Bunder, Roberts, and Kevrekidis (2017a) studied the patch scheme for 1D heterogeneous diffusion and showed accurate coupling conditions should take account of the underlying microscale structure with the interpolation between points strictly controlled by the period of the heterogeneous diffusion. Although the coupling conditions constructed by Bunder, Roberts, and Kevrekidis (2017a) were shown to be effective for 1D heterogeneous diffusion, as were similar coupling conditions for many other systems (Roberts, MacKenzie, and Bunder 2013; Cao and Roberts 2015; Jarrad and Roberts 2018), these coupling conditions fail to preserve self-adjoint symmetry and thus do not maintain a fundamental symmetry of the original problem. A system represented by $\partial_t \mathbf{u} = \mathcal{L}\mathbf{u}$ with field \mathbf{u} and linear operator \mathcal{L} is defined to be *self-adjoint* if for all fields \mathbf{v}, \mathbf{u} , \mathcal{L} satisfies $\langle \mathbf{u}, \mathcal{L}\mathbf{v} \rangle = \langle \mathcal{L}\mathbf{u}, \mathbf{v} \rangle$ for some inner product. Here, we consider lattice systems with square matrix operator \mathcal{L} and apply the usual complex inner product $\langle \mathbf{u}, \mathbf{v} \rangle = \mathbf{u}^\dagger \mathbf{v}$, where \dagger denotes the complex conjugate transpose. To ensure that operator \mathcal{L} is self-adjoint it must satisfy $\mathcal{L}^\dagger = \mathcal{L}$, termed *Hermitian*.¹ An approximation scheme which does not maintain self-adjoint symmetry may result in a solution which does not satisfy essential requirements, such as conservation of energy. In particular, generalising the 1D patch scheme for heterogeneous diffusion developed by Bunder, Roberts, and Kevrekidis (2017a) to 2D heterogeneous diffusion produces undesirable fluctuations in the simulation. These fluctuations arise because such a 2D patch system produces a non-self-adjoint Jacobian that possessed complex eigenvalues. Here we construct new patch coupling conditions which maintain the self-adjoint symmetry of the original microscale system, for both 1D and 2D space. By preserving self-adjoint symmetry, these new coupling conditions have much wider applicability.

The code developed herein now forms part of a flexible MATLAB/Octave Toolbox (Maclean, Bunder, and Roberts 2020) for equation-free computations that any researcher can download and use for a variety of problems (Roberts, Maclean, and Bunder 2020). This Toolbox provides equation-free code

¹Often \mathcal{L} is a real matrix, and then this Hermitian property is the usual matrix symmetry.

suitable for many systems, such as diffusion and wave dynamics, and grants the user full flexibility in selecting one of the supplied projective integration and/or patch coupling schemes or importing user-written code.

To clarify the theoretical results and demonstrate the benefits of our novel self-adjoint patch scheme we use the examples of 1D and 2D microscale heterogeneous diffusion (Sections 2 and 3, and Section 4, respectively). For the 2D case we pose that the system’s evolving variables $\mathbf{u}_{i,j}(\mathbf{t})$ are defined on a spatial lattice of points (x_i, y_j) with microscale spacing \mathbf{d} ($\Delta x_i = \Delta y_j = \mathbf{d}$) and indexed by integers i, j . The governing large set of ODEs of the heterogeneous diffusion is then

$$\begin{aligned} \mathbf{d}^2 \partial_t \mathbf{u}_{i,j} = & \kappa_{i+\frac{1}{2},j}(\mathbf{u}_{i+1,j} - \mathbf{u}_{i,j}) + \kappa_{i-\frac{1}{2},j}(\mathbf{u}_{i-1,j} - \mathbf{u}_{i,j}) \\ & + \kappa_{i,j+\frac{1}{2}}(\mathbf{u}_{i,j+1} - \mathbf{u}_{i,j}) + \kappa_{i,j-\frac{1}{2}}(\mathbf{u}_{i,j-1} - \mathbf{u}_{i,j}) \end{aligned} \quad (1)$$

for heterogeneous diffusivities $\kappa_{i,j}$ which vary periodically over the given domain. Figure 1 illustrates such a lattice, albeit restricted to patches in space rather than space-time. Here, for clarity of notation, and as shown in the figure, we assume a square domain and a square microscale lattice, but Section 4 generalises to a rectangular domain and rectangular microscale lattice. We use the relatively simple example of heterogeneous diffusion as it is a canonical example which describes many physical systems and naturally extends to more complex systems, such as wave propagation and advection-diffusion, as briefly discussed in Section 2.3.

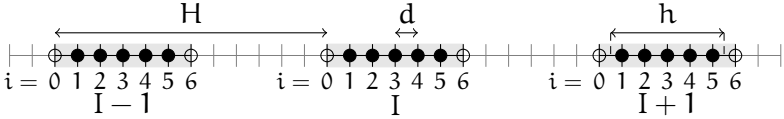
There are many multiscale methods which would provide good solutions to multiscale heterogeneous systems such as (1), as reviewed by both Engquist and Souganidis (2008) and Saeb, Steinmann, and Javili (2016). For example, Abdulle and Grote (2011) and Engquist, Holst, and Runborg (2011) applied the heterogeneous multi-scale method (HMM) to wave propagation in heterogeneous media, although it is predicated on an infinitely large scale separation between the ‘slow’ variables which persist at the macroscale and the ‘fast’ variables which are only observable at the microscale. Maier and Peterseim (2019) and Peterseim (2019) considered a similar wave propagation model, but avoided the need for infinite scale separations by applying localized orthogonal decomposition with numerical homogenization. Romanazzi,

Bruna, and Howey (2016) also applied HMM to compute a macroscale model for a heterogeneous system of closely packed insulated conductors. Owhadi (2015) investigated heterogeneous diffusion with numerical homogenization, but reformulated it as a Bayesian inference problem, thus providing a new methodology for deriving basis elements of the microscale structure. Cornaggia and Guzina (2020) considered one-dimensional waves in periodic media and derived homogenized boundary and transmission conditions in the usual separation of scales infinite limit. Homogenization and HMM multi-scale models rely on being able to identify ‘fast’ and ‘slow’ variables in the microscale model and some prior knowledge of the macroscale model, and generally these models require substantial analytic work prior to numerical implementation (Carr, Perré, and Turner 2016) while also relying on an infinite separation of scales. In contrast, equation-free modelling makes no assumptions concerning fast and slow variables, needs no limit on the separation of scales, and requires no knowledge of the macroscale model, but instead computes a numerical macroscale solution on-the-fly. Consequently, equation-free modelling provides macroscale system-level predictions for complex dynamical systems which cannot be solved via other schemes.

2 Self-adjoint preserving patch scheme for 1D

The general scenario is when scientists or engineers has a well-specified microscale system on a characteristic microscale length d , but are only interested in the behaviour of this system at some significantly larger macroscale $H \gg d$. An important class of examples is the prediction of the macroscale, homogenised, dynamics of the microscale heterogeneous diffusion of a field $u(x, t)$ satisfying the PDE $\partial_t u = \partial_x[\kappa(x)\partial_x u]$ where the diffusivity varies rapidly on the length-scale d (Engquist and Souganidis 2008; Saeb, Steinmann, and Javili 2016; Bunder, Roberts, and Kevrekidis 2017a, e.g.). A distinguishing feature of our patch dynamics approach is that we do *not* require infinite scale separation “ $d \rightarrow 0$ ”; instead the methodology applies at finite d via supporting theory which is directly applicable to finite d (c.f., Engquist and Souganidis 2008, who apply scale separation $\epsilon \rightarrow 0$).

Figure 2: three 1D spatial patches indexed by I and $I \pm 1$. Filled circles indicate patch interior points with microscale spacing d , and unfilled circles represent patch edge points. The gaps between patches are unsimulated space. These patches have $n = 5$ interior points indexed by $i = 1 : n$, and the two edges have indices $i = 0$ and $i = n + 1 = 6$. The macroscale spacing between patches is H , and the width of each patch is denoted $h := nd$, as shown.



For simplicity, we introduce our approach for systems defined on a microscale spatial lattice, such as a spatial discretisations of PDEs on the microscale length d . This section introduces how to construct patches for a 1D system so that a computational simulation on these patches efficiently and accurately predicts the macroscale of interest without needing to derive a macroscale closure. In this patch construction we focus on the specific example of 1D heterogeneous diffusion on a microscale lattice, but the new patch scheme is similar for a wide range of 1D systems, including nonlinear systems (e.g., via the toolbox by Maclean, Bunder, and Roberts 2020).

In 1D, the lattice has points x_i of microscale spacing d and we seek to predict the dynamics of the variables $u_i(t)$. Heterogeneous diffusion on this 1D microscale lattice is the restriction of (1), namely

$$d^2 \partial_t u_i = \kappa_{i+\frac{1}{2}} (u_{i+1} - u_i) + \kappa_{i-\frac{1}{2}} (u_{i-1} - u_i). \quad (2)$$

As illustrated in Figure 2, to implement the 1D patch scheme we construct N small patches across the spatial domain, separated by macroscale length H and indexed by $I = 1, 2, \dots, N$. Generally we use uppercase letters to denote macroscale quantities, and lowercase letter to denote microscale quantities. Each patch has n *interior* microscale points indexed by $i = 1 : n$ (herein, $k : \ell$ denotes $k, k + 1, k + 2, \dots, \ell$) and *two edge* points indexed by $i = 0$ on the left and $i = n + 1$ on the right: in the I th patch the location of these points is denoted by x_i^I . We call n the *size* of the patches, as opposed

to the physical patch *width* h . We now relabel the microscale field values, using \mathbf{u}_i^I to denote the value of \mathbf{u} in patch I at microscale patch interior index i . Similarly, $\kappa_{i+1/2}^I$ is the diffusivity between the i and $i+1$ points in the I th patch. The patch scheme uses the given microscale system (2) inside each patch (as a given ‘black-box’), here the sub-patch ODEs are

$$d^2 \partial_t \mathbf{u}_i^I = \kappa_{i+1/2}^I (\mathbf{u}_{i+1}^I - \mathbf{u}_i^I) + \kappa_{i-1/2}^I (\mathbf{u}_{i-1}^I - \mathbf{u}_i^I), \quad (3)$$

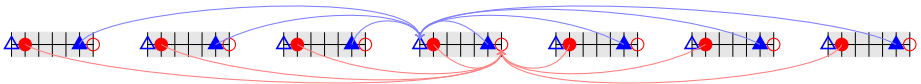
on the interior points $i = 1 : n$ for every patch I, where ‘sub-patch’ refers to spatial scales less than the patch width h . These patches are coupled together by setting the patch-edge values \mathbf{u}_0^I and \mathbf{u}_{n+1}^I through interpolation of \mathbf{u} -values from neighbouring patches (Figure 3). The new scheme is to interpolate from the interior values closest to the patch edges, the next-to-edge values \mathbf{u}_1^I and \mathbf{u}_n^I , to determine the edge values \mathbf{u}_{n+1}^I and \mathbf{u}_0^I , respectively. As illustrated in Figure 3, the interpolation is from the *opposite* patch edge so that \mathbf{u} -values at $i = 1$ in nearby patches I are interpolated to the edge \mathbf{u} -value at $i = n + 1$, and \mathbf{u} -values at $i = n$ in nearby patches I are interpolated to the edge \mathbf{u} -value at $i = 0$.

This article establishes that this new patch scheme both preserves self-adjoint symmetry and also accurately captures the macroscale behaviour of the full heterogeneous system (2).

This self-adjoint coupling is analogous to that applied by Gear, Li, and Kevrekidis (2003) in a gap-tooth method particle simulation. In their particle simulation, at the right edge of patch I, some fraction $\alpha \leq 1$ of the right-moving particles (i.e., those particles leaving patch I via the right edge) enter the left edge of adjacent patch I + 1, and the remaining fraction $1 - \alpha$ enter the left edge of patch I. Similarly, left-moving particles at the left edge of patch I (i.e., those particles leaving patch I via the left edge) are either distributed to the right edge of patch I - 1 or to the right edge of patch I. Gear, Li, and Kevrekidis (2003) justified their coupling using a flux analogy.

The patch width $h := n d$ is measured across the interior points from/to midway between the extreme pairs of microscale points (Figure 2). The crucial ratio $r := h/H$ is, in 1D, the fraction of the given spatial domain on which microscale computation takes place. For efficient simulations

Figure 3: patch self-adjoint preserving coupling. Filled triangles/circles at indices $i = n, 1$ represent next-to-edge points whose u -values are interpolated to give u -values at the edge points, $i = 0, n + 1$, represented by unfilled triangles/circles. Interpolation to the left/right edge of a patch is from the next-to-edge points on the right/left of nearby patches, as indicated by blue/red arrows.



we typically choose ratio $r \ll 1$, equivalently $h \ll H$. Herein, examples illustrating system-level predictions often use $r = 0.1$ so that there is a significant proportion of uncomputed space—the patch scheme is a sparse simulation; however, in example simulations (e.g., Figures 1 and 4), for better visualisation we often choose larger r . When the ratio $r = 1$ the patch scheme computes the given microscale system, here (2), since the left edge $i = 0$ of the I th patch coincides with the $i = n$ next-to-edge point of the $(I - 1)$ th patch, and the right edge $i = n + 1$ of the I th patch coincides with the $i = 1$ next-to-edge point of the $(I + 1)$ th patch, and thus the patches cover all microscale points in the domain. Sections 2.2 to 2.4 demonstrate here, and Section 3 proves in general, that patches with small fraction r accurately predict the macroscale dynamics.

2.1 Self-adjoint patch coupling for 1D

A key requirement in accurate patch simulations is carefully chosen patch coupling. Most previous patch implementations (e.g., Roberts, MacKenzie, and Bunder 2013; Cao and Roberts 2015; Bunder, Roberts, and Kevrekidis 2017a) interpolated the u -values from the centre of each patch to determine the u -values on the patch edges. This was proven to be accurate for smooth dynamics in both 1D and 2D, as well as for 1D heterogeneous diffusion (Bunder, Roberts, and Kevrekidis 2017a). However, this centre interpolated coupling scheme has one weakness: it does not preserve the self-adjoint nature, the

symmetry, of many physical systems, such as the diffusion (2). This section establishes, via Lemmas 1 and 3, that our new patch coupling (Figure 3) preserves the self-adjoint symmetry of the original microscale system.

The dynamic variables in the patch scheme are the \mathbf{u} -values at the interior points of the patches. Hence, for every patch I , denote the vector of interior values by $\mathbf{u}^I := (\mathbf{u}_1^I, \dots, \mathbf{u}_n^I) \in \mathbb{R}^n$. These vectors do not contain the patch edge values \mathbf{u}_0^I and \mathbf{u}_{n+1}^I because edge values are determined by interpolation from nearby patches. Denote the global \mathbf{u} -values by the vector $\mathbf{u} := (\mathbf{u}^1, \dots, \mathbf{u}^N) \in \mathbb{R}^{nN}$. Then the microscale linear diffusion (3) on the coupled patches has the form of the linear systems of ODES

$$\partial_t \mathbf{u} = \mathcal{L} \mathbf{u}, \quad (4)$$

for real-valued $nN \times nN$ matrix \mathcal{L} . From the patch structure, the square matrix \mathcal{L} has the form of $N \times N$ blocks, each of microscale size $n \times n$. Let \mathcal{L}^{IJ} be the $n \times n$ block of the influence on patch I from patch J . Here, for heterogeneous systems such as (3), we establish that the inter-patch coupling shown by Figure 3 ensures that \mathcal{L} is self-adjoint, which in turn ensures accurate macroscale predictions. As discussed in Section 1, \mathcal{L} is self-adjoint when it is equal to its Hermitian conjugate, $\mathcal{L} = \mathcal{L}^\dagger$, and so when \mathcal{L} is real we only require it to be symmetric.

One crucial proviso for these results is that the patch width $h = nd$ must be an integral multiple of the period of the microscale heterogeneity. The desirability of such a limitation on the patch width has been observed before (Bunder, Roberts, and Kevrekidis 2017b, §5.2) (Abdulle, Arjmand, and Paganoni 2020, p.3, Ref. 5, 19, 20, e.g.) (Abdulle et al. 2012, p.62). However, Section 2.4 shows that, and Section 3.1 proves that, embedding the given heterogeneous system into an ensemble overcomes this limitation on the patch width.

We decompose the matrix in (4) into two parts, $\mathcal{L} = \mathcal{D} + \mathcal{C}$, for block diagonal dynamics matrix $\mathcal{D} = [\mathcal{D}^I]$ and coupling matrix $\mathcal{C} = [\mathcal{C}^{IJ}]$ with $n \times n$ blocks \mathcal{D}^I and \mathcal{C}^{IJ} . For \mathcal{L} to be self-adjoint requires that both \mathcal{D} and \mathcal{C} are self-adjoint, that is, $(\mathcal{D}^I)^\dagger = \mathcal{D}^I$ and $(\mathcal{C}^{IJ})^\dagger = \mathcal{C}^{JI}$. The blocks of the dynamics matrix \mathcal{D}^I encode the given sub-patch ODES (3) within the I th patch, and

without any patch coupling. Thus \mathcal{D} is self-adjoint if the given microscale system is self-adjoint. For example, for 1D microscale diffusion ODEs (3) the elements of the dynamics matrix are, for every patch I ,

$$\begin{aligned} \mathcal{D}_{i,i}^I &= -\kappa_{i+\frac{1}{2}}^I - \kappa_{i-\frac{1}{2}}^I & \text{for } i = 1 : n, \\ \mathcal{D}_{i,i+1}^I &= \mathcal{D}_{i+1,i}^I = \kappa_{i+\frac{1}{2}}^I & \text{for } i = 1 : n-1, \end{aligned} \quad (5)$$

and therefore \mathcal{D} is symmetric and real, and thus self-adjoint.

We now construct a self-adjoint coupling matrix \mathcal{C} specifically for 1D heterogeneous diffusion (3), but readily adaptable to any 1D system of second order in space. We make the following two assumptions that reflect that we want the sub-patch system to be almost a ‘black-box’.

A1 The microscale ODEs (3) are unmodified for all i and I .

A2 The patch edge values \mathbf{u}_0^I and \mathbf{u}_{n+1}^I are determined by an interpolation that is independent of the diffusion coefficients.

Assumption A1 requires that rows $i = 2 : n-1$ of \mathcal{C}^{IJ} must be zero because \mathcal{D}^I already encodes the ODEs (3) for $i = 2 : n-1$. Consequently, since symmetry requires $\mathcal{C}^{IJ} = (\mathcal{C}^{JI})^\dagger$, the columns $j = 2 : n-1$ must be zero. Thus the only nonzero elements in \mathcal{C}^{IJ} are the four corner elements \mathcal{C}_{ij}^{IJ} for $i, j = 1, n$. Given the form of \mathcal{D} in (5), and the form of the ODEs (3), to satisfy **Assumption A1** for the two cases $i = 1, n$ we must have

$$\kappa_{\frac{1}{2}}^I \mathbf{u}_0^I = \sum_J (\mathcal{C}_{11}^{IJ} \mathbf{u}_1^J + \mathcal{C}_{1n}^{IJ} \mathbf{u}_n^J) \quad \text{and} \quad \kappa_{n+\frac{1}{2}}^I \mathbf{u}_{n+1}^I = \sum_J (\mathcal{C}_{n1}^{IJ} \mathbf{u}_1^J + \mathcal{C}_{nn}^{IJ} \mathbf{u}_n^J). \quad (6)$$

These two equations couple patches across the unsimulated space between patches by setting the two patch edge values \mathbf{u}_0^I and \mathbf{u}_{n+1}^I as interpolations of the sub-patch fields \mathbf{u}_1^I and \mathbf{u}_n^I .

To satisfy **Assumption A2** we introduce an $nN \times nN$ *interpolation* matrix \mathcal{I} that has no dependence on the diffusion coefficients, with the same block structure as \mathcal{C} where $\mathcal{I}_{ij}^{IJ} := 0$ for i or $j \neq 1, n$, whereas for $j = 1, n$ the entries satisfy $\mathcal{C}_{1j}^{IJ} = \kappa_{1/2}^I \mathcal{I}_{1j}^{IJ}$ and $\mathcal{C}_{nj}^{IJ} = \kappa_{n+1/2}^I \mathcal{I}_{nj}^{IJ}$. Consequently, (6) simplifies so

that the interpolation to the patch-edge values is independent of the diffusion coefficients:

$$\mathbf{u}_0^I = \sum_J (\mathcal{I}_{11}^{IJ} \mathbf{u}_1^J + \mathcal{I}_{1n}^{IJ} \mathbf{u}_n^J) \quad \text{and} \quad \mathbf{u}_{n+1}^I = \sum_J (\mathcal{I}_{n1}^{IJ} \mathbf{u}_1^J + \mathcal{I}_{nn}^{IJ} \mathbf{u}_n^J).$$

For the interpolation to generically interpolate real-values to real-values we thus require matrix \mathcal{I} , and hence \mathcal{C} , to be real. But we have not yet completely ensured \mathcal{C} is self-adjoint.

For \mathcal{C} to be self-adjoint we require that $\mathcal{C}_{1n}^{IJ} = \kappa_{1/2}^I \mathcal{I}_{n1}^{IJ} = \mathcal{C}_{n1}^{JI} = \kappa_{n+1/2}^J \mathcal{I}_{1n}^{JI}$, $\mathcal{C}_{11}^{IJ} = \kappa_{1/2}^I \mathcal{I}_{11}^{IJ} = \mathcal{C}_{11}^{JI} = \kappa_{1/2}^J \mathcal{I}_{11}^{JI}$ and $\mathcal{C}_{nn}^{IJ} = \kappa_{n+1/2}^I \mathcal{I}_{nn}^{IJ} = \mathcal{C}_{nn}^{JI} = \kappa_{n+1/2}^J \mathcal{I}_{nn}^{JI}$, and since the interpolation coefficients are independent of the diffusion they must satisfy $\mathcal{I}_{1n}^{IJ} = \mathcal{I}_{n1}^{JI}$, $\mathcal{I}_{11}^{IJ} = \mathcal{I}_{11}^{JI}$ and $\mathcal{I}_{nn}^{IJ} = \mathcal{I}_{nn}^{JI}$. But if the interpolation matrix ‘top-left’ and ‘bottom-right’ elements \mathcal{I}_{11}^{IJ} and \mathcal{I}_{nn}^{IJ} are nonzero, then they cannot produce an accurate interpolation. To see why, say $J \geq I$ so that \mathbf{u}_1^J is a distance of $H(J - I) + d$ from \mathbf{u}_0^I , and \mathbf{u}_1^I is a distance of $H(J - I) - d$ from \mathbf{u}_0^I —these different distances imply that if coefficients \mathcal{I}_{11}^{IJ} and \mathcal{I}_{11}^{JI} are nonzero, then they should not have the same magnitude. A similar argument implies that nonzero \mathcal{I}_{nn}^{IJ} and \mathcal{I}_{nn}^{JI} should not have the same magnitude. Thus we set $\mathcal{I}_{11}^{IJ} = \mathcal{I}_{nn}^{IJ} = 0$. Consequently, the only coupling entries which may be nonzero are $\kappa_{1/2}^I \mathcal{I}_{n1}^{IJ} = \kappa_{n+1/2}^J \mathcal{I}_{1n}^{JI}$, and for $\mathcal{I}_{n1}^{IJ} = \mathcal{I}_{1n}^{JI}$ our diffusion is then constrained by $\kappa_{1/2}^I = \kappa_{n+1/2}^J$ for all patches I, J . The resulting interpolation gives edge values

$$\mathbf{u}_0^I = \sum_J \mathcal{I}_{1n}^{IJ} \mathbf{u}_n^J \quad \text{and} \quad \mathbf{u}_{n+1}^I = \sum_J \mathcal{I}_{n1}^{IJ} \mathbf{u}_1^J. \quad (7)$$

Figure 3 draws this interpolation and shows that for symmetric interpolation matrix \mathcal{I} the interpolation is implemented with both translational and rotational symmetry (i.e., interpolations are invariant upon reflection and swapping red-blue).

Thus Assumption A1 and Assumption A2 not only tightly constrain the form of coupling matrix \mathcal{C} , they also constrain the patch size and placement by requiring that the diffusivities satisfy $\kappa_{1/2}^I = \kappa_{n+1/2}^J$ for every patch I, J . If the heterogeneity is periodic, period p , then this constrains the patch

width h by requiring the number of patch interior indices n to be divisible by the heterogeneous period p . Section 2.4 shows that this constraint on the patch width may be overcome by embedding the diffusion into an ensemble of phase-shifted diffusions, but as this embedding increases the size of the simulation by a factor of p , it incurs extra computation and so might not be suitable for all applications.

The self-adjoint matrix operator \mathcal{L} is here developed in the context of 1D heterogeneous diffusion. Nonetheless, the same coupling matrix \mathcal{C} could be used for any system where the dynamics matrix \mathcal{D} is self-adjoint and the given microscale model is no more than second order in space, and thus requiring only one coupling condition on each patch edge. Higher order microscale models, for example, microscale models fourth order in space, require two coupling conditions for each patch edge and therefore require a more complicated coupling matrix \mathcal{C} .

Section 2.2 discusses the case of global spectral coupling, whereas Section 2.3 discusses coupling from a finite number of near neighbouring patches. Such patch couplings have different coupling matrices \mathcal{C} , but for both $\mathcal{L} = \mathcal{D} + \mathcal{C}$ is self-adjoint, and both satisfy Assumption A1 and Assumption A2.

2.2 Spectral coupling of patches

This coupling uses a spectral interpolation of selected patch interior values to give the values on patch edges. Here we assume the macroscale solution is L -periodic in space, for domain length $L := NH$. This spectral coupling is very accurate, as indicated by consistency arguments in Section 3 and by numerical tests in Section 4.1 for the 2D case which also hold in 1D.

Let's start by determining the patches' right-edge values \mathbf{u}_{n+1}^I . The first step is to compute the Fourier transform, the N coefficients \mathbf{u}_k , of the left-next-to-edge values \mathbf{u}_1^I (the over-harpoon to the right denotes using left-values to determine right-values). That is, recalling x_1^I is the spatial location of \mathbf{u}_1^I ,

the Fourier transform computes the coefficients ($i := \sqrt{-1}$)

$$\vec{u}_k := \frac{1}{N} \sum_I u_1^I e^{-ikx_1^I}, \quad \text{so that } u_1^I = \sum_k \vec{u}_k e^{ikx_1^I}, \quad I = 1 : N. \quad (8a)$$

The wavenumbers k in these Fourier transforms are an appropriate fixed set of integer multiples of $2\pi/L$ for domain length L . The second step computes the right-edge values by evaluating this Fourier transform at the right-edge of each patch, namely at $x_{n+1}^I = x_1^I + h$ for the displacement of one patch width $h = nd$. Hence

$$u_{n+1}^I := \sum_k \vec{u}_k e^{ikx_{n+1}^I} = \sum_k \vec{u}_k e^{ik(x_1^I + h)} = \sum_k (\vec{u}_k e^{ikh}) e^{ikx_1^I}, \quad (8b)$$

which is efficiently realised by computing the inverse Fourier transform of the values $\vec{u}_k e^{ikh}$ for the range of wavenumbers k .

Similarly, to compute left-edge values u_0^I a Fourier transform computes the coefficients \vec{u}_k of the right-next-to-edge values u_n^I using the same set of wavenumbers, shifts a displacement $-h$ by multiplying by e^{-ikh} , and then an inverse Fourier transform interpolates to the patch left-edge: from the Fourier transform

$$u_n^I = \sum_k \vec{u}_k e^{ikx_n^I}, \quad \text{then } u_0^I := \sum_k (\vec{u}_k e^{-ikh}) e^{ikx_n^I}. \quad (8c)$$

Lemma 1. *Coupling patches with the spectral interpolation (8) preserves the self-adjoint symmetry of heterogeneous systems in the form (3).*

Some algebra now establishes this lemma. The effect of the spectral interpolation to the right-edge is, recalling the patch-width $h = rH$,

$$\begin{aligned} u_{n+1}^I &:= \sum_k \vec{u}_k e^{ikh} e^{ikx_1^I} = \sum_k \frac{1}{N} \sum_J u_1^J e^{-ikx_1^J} e^{ikh} e^{ikx_1^I} \\ &= \sum_J u_1^J \sum_k \frac{1}{N} e^{ik(-x_1^J + h + x_1^I)} = \sum_J u_1^J \sum_k \frac{1}{N} e^{ikH(I-J+r)} \end{aligned}$$

$$= \sum_J \mathcal{I}_{n1}^{IJ} \mathbf{u}_1^J \quad \text{for } \mathcal{I}_{n1}^{IJ} := \frac{1}{N} \sum_k e^{ikH(I-J+r)}. \quad (9a)$$

Similarly, the effect of the spectral interpolation to the left-edge is

$$\mathbf{u}_0^I = \dots = \sum_J \mathcal{I}_{1n}^{IJ} \mathbf{u}_n^J \quad \text{for } \mathcal{I}_{1n}^{IJ} := \frac{1}{N} \sum_k e^{ikH(I-J-r)}. \quad (9b)$$

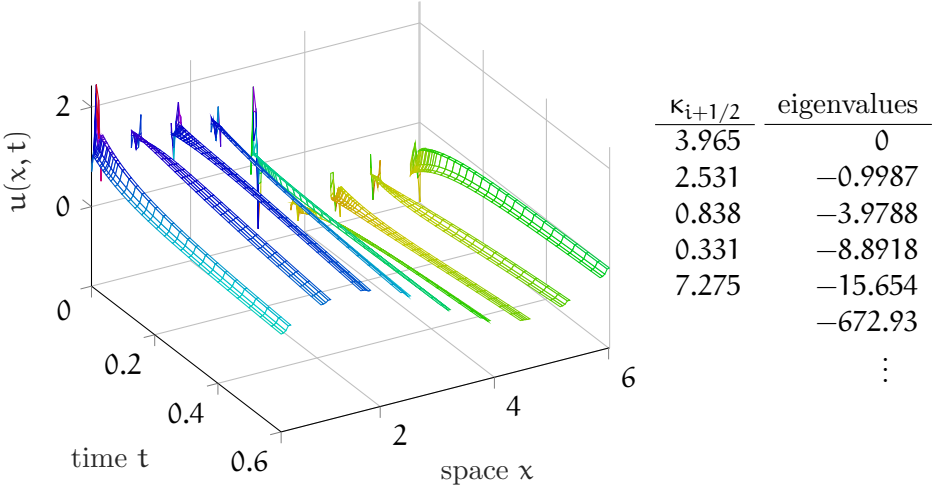
These expressions determine the coefficients in the coupling matrix \mathcal{C} .

Since the sums in (9) all use the same set of wavenumbers k , then every pair of interpolation matrix elements \mathcal{I}_{1n}^{IJ} and \mathcal{I}_{n1}^{JI} are the complex conjugate of each other. In real problems, provided every wavenumber k in these Fourier sums is partnered by the corresponding negative wavenumber $-k$ in the sum (as is usual), then the complex sums for \mathcal{I}_{1n}^{IJ} and \mathcal{I}_{n1}^{JI} are all real-valued, and since they are complex conjugates they must be equal, $\mathcal{I}_{1n}^{IJ} = \mathcal{I}_{n1}^{JI}$. Hence, \mathcal{C} is symmetric and so this spectral coupling preserves self-adjoint symmetry.

Figure 4 shows one example patch simulation in space-time of the heterogeneous diffusion (3). In the initial condition at time $t = 0$ the ragged sub-patch structure is rapidly smoothed within each patch—the remaining sub-patch structure is due to the heterogeneous diffusion. Then the patches evolve over the shown macroscale time with the macroscale mode $\mathbf{u} \propto \sin x$ decaying slowest as appropriate.

Remark 2 (Hilbert space generalisation). Our discussion predominantly addresses the case where the field values $\mathbf{u}_i \in \mathbb{R}$. However, the arguments equally well apply to cases where the field values \mathbf{u}_i are in a Hilbert space, say denoted \mathbb{H} . In that case the diffusivities $\kappa_{i+1/2}$ are to be interpreted as linear operators $\kappa_{i+1/2} : \mathbb{H} \rightarrow \mathbb{H}$, and the discourse appropriately rephrased—provided the operators are suitable. Such a generalisation empowers much wider applicability of the results we establish, but for simplicity we mainly focus on the basic case of real \mathbf{u}_i . Nonetheless, Section 2.4 introduces an ensemble of phase-shifted diffusions whose analysis requires the case of \mathbf{u}_i being in the Hilbert space of \mathbb{R}^P , and similarly in Section 4.

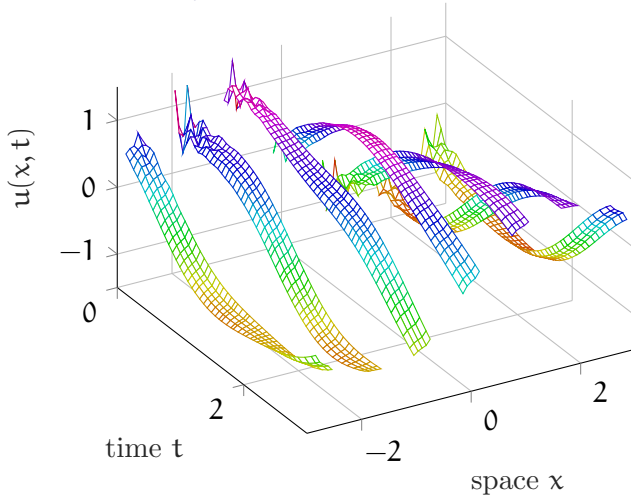
Figure 4: example simulation in 1D space of heterogeneous diffusion (3) on nine patches with spectral coupling (8) and rather large size ratio $r = 0.3$ (for visibility). The listed diffusion coefficients $\kappa_{i+1/2}$ have period five, and each patch has $n = 5$ interior points as plotted. The first five computed eigenvalues of the scheme’s operator \mathcal{L} are expectedly close to $-k^2$, and then have a large spectral gap to the sub-patch modes.



2.3 Lagrangian spatial coupling of patches

Spectral coupling constructs a single Fourier interpolant through all patches and then use this one interpolant to compute the edge values of each patch; thus the coupling matrix elements \mathcal{C}_{1n}^{IJ} and \mathcal{C}_{n1}^{IJ} are nonzero for every patch I and J—it is a global coupling. An alternative local scheme is, for each patch, to construct an interpolant from neighbouring patches so that the inter-patch coupling occurs only over a finite local region of the spatial domain. Such Lagrangian, or polynomial, coupling is the most common form to date (e.g., Roberts, MacKenzie, and Bunder 2013; Cao and Roberts 2015; Bunder, Roberts, and Kevrekidis 2017a), but has always been constructed by interpolation of the fields (or field averages) from the centre of each patch—a scheme which does not generally maintain self-adjoint symmetry. In

Figure 5: patch simulation, with quadratic coupling, of ‘weakly damped’ waves on a heterogeneous lattice illustrates the emergence of a coherent travelling macroscale wave from a noisy initial condition: in terms of the microscale difference operator δ_i (Table 1), the system is $du_i/dt = v_i$, $dv_i/dt = \delta_i(\kappa_i\delta_i u_i) + 0.02\delta_i^2 v_i$ for log-normal κ_i .



contrast, our scheme to couple via next-to-edge values preserves self-adjoint symmetry. Consequently, sensitive simulations such as the propagating waves of Figure 5 preserve physically desirable properties, even with low-order coupling (here quadratic), and for propagation through this microscale heterogeneous medium.

To develop the Lagrangian coupling, here we adapt the derivation of Bunder, Roberts, and Kevrekidis (2017a) to the constraints identified by Section 2.1 for self-adjoint coupling. Define a macroscale step operator E which shifts a field by one macroscale step H to the right: $E u_i^I = u_i^{I+1}$. Its inverse shifts by one macroscale step to the left: $E^{-1} u_i^I = u_i^{I-1}$. Define standard macroscale mean and difference operators, $\mu := (E^{1/2} + E^{-1/2})/2$ and $\delta := E^{1/2} - E^{-1/2}$, respectively. These three operators are related by $\mu^2 = 1 + \frac{1}{4}\delta^2$ and $E^{\pm 1} = 1 \pm \mu\delta + \frac{1}{2}\delta^2$. When operating on a field u_i^I , the mean and

difference operators involve patches to the left and right of patch I; for example, $\mu\delta u_i^I = (u_i^{I+1} - u_i^{I-1})/2$ and $\delta^2 u_i^I = u_i^{I+1} - 2u_i^I + u_i^{I-1}$, and for every positive exponent K the operators $\mu\delta^{2K-1} u_i^I$ and $\delta^{2K} u_i^I$ involve patch values $u_i^I, u_i^{I\pm 1}, \dots, u_i^{I\pm K}$.

To construct the Lagrangian self-adjoint coupling, we write the edge values in terms of known next-to-edge values for patches J near patch I. Define P as the number of coupled nearest neighbours to the left and right of each patch I. That is, patch I is coupled to the $2P + 1$ closest patches, including itself, and wrapped periodically for the case of macroscale periodicity, thus forming an effective local coupling stencil of physical width $(2P + 1)H$. For patch I, the right-edge u_{n+1}^I is a distance $h = nd = rH$ from the left-next-to-edge u_1^I . Consequently, in terms of the fractional macroscale shift E^r , $u_{n+1}^I = E^r u_1^I$ determines the right-edge value by interpolating the left-next-to-edge values. We expand the fractional shift, in powers of δ up to order $2P$, via $E^r = (1 + \mu\delta + \frac{1}{2}\delta^2)^r$, where powers of μ are removed via the identity $\mu^2 = 1 + \frac{1}{4}\delta^2$. Then the right-edge values are computed as

$$u_{n+1}^I = E^r u_1^I \approx u_1^I + \sum_{k=1}^P \left(\prod_{\ell=0}^{k-1} (r^2 - \ell^2) \right) \frac{+(2k/r)\mu\delta^{2k-1} + \delta^{2k}}{(2k)!} u_1^I. \quad (10a)$$

Similarly for the left-edge values, with the difference that the fractional shift is E^{-r} from the right-next-to-edge, so that left-edge values are computed as

$$u_0^I = E^{-r} u_n^I \approx u_n^I + \sum_{k=1}^P \left(\prod_{\ell=0}^{k-1} (r^2 - \ell^2) \right) \frac{-(2k/r)\mu\delta^{2k-1} + \delta^{2k}}{(2k)!} u_n^I. \quad (10b)$$

The highest-order operators are $\mu\delta^{2P-1}$ and δ^{2P} , and thus the above expressions involve patches J where J is no more than P from patch I. The coefficients of u_1^J, u_n^J in the interpolations (10) define the interpolation matrix elements $\mathcal{I}_{n1}^{IJ}, \mathcal{I}_{1n}^{IJ}$, respectively, as in (7), for patches I and J no more than P apart. For greater distances between the two patches $\mathcal{I}_{n1}^{IJ} = \mathcal{I}_{1n}^{IJ} = 0$.

Section 2.1 shows that self-adjoint coupling requires symmetry $\mathcal{I}_{n1}^{IJ} = \mathcal{I}_{1n}^{JI}$ (all elements are real so there is no need to involve the complex conjugate). The coupling conditions (10) satisfy this symmetry constraint via the r dependence

of the interpolation matrix elements: $\mathcal{I}_{n1}^{\text{IJ}}(\mathbf{r}) = \mathcal{I}_{n1}^{\text{II}}(-\mathbf{r}) = \mathcal{I}_{1n}^{\text{IJ}}(-\mathbf{r}) = \mathcal{I}_{1n}^{\text{II}}(\mathbf{r})$. For example, for only nearest neighbour coupling with $\mathbf{P} = 1$, the interpolations (10) give

$$\begin{aligned} \mathbf{u}_{n+1}^{\text{I}} &= \frac{r}{2}(\mathbf{r} - 1)\mathbf{u}_1^{\text{I}^{-1}} + (1 - r^2)\mathbf{u}_1^{\text{I}} + \frac{r}{2}(\mathbf{r} + 1)\mathbf{u}_1^{\text{I}^{+1}}, \\ \mathbf{u}_0^{\text{I}} &= \frac{r}{2}(\mathbf{r} + 1)\mathbf{u}_n^{\text{I}^{-1}} + (1 - r^2)\mathbf{u}_n^{\text{I}} + \frac{r}{2}(\mathbf{r} - 1)\mathbf{u}_n^{\text{I}^{+1}}, \end{aligned}$$

so, for every patch I, $\mathcal{I}_{n1}^{\text{I},\text{I}^{-1}} = \frac{r}{2}(\mathbf{r} - 1) = \mathcal{I}_{1n}^{\text{I}^{-1},\text{I}}$, $\mathcal{I}_{n1}^{\text{I},\text{I}^{+1}} = \frac{r}{2}(\mathbf{r} + 1) = \mathcal{I}_{1n}^{\text{I}^{+1},\text{I}}$, and $\mathcal{I}_{n1}^{\text{II}} = 1 - r^2 = \mathcal{I}_{1n}^{\text{II}}$. Thus the above derivation establishes the following lemma.

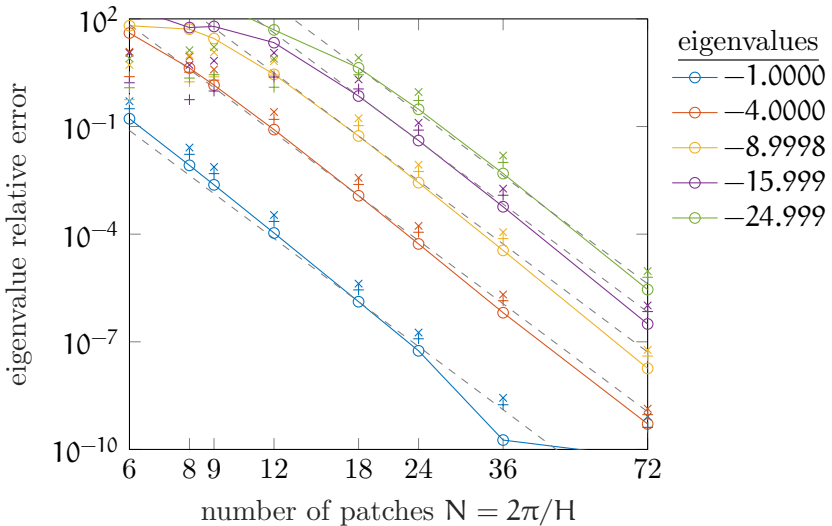
Lemma 3. *For every order \mathbf{P} , coupling patches with the Lagrangian interpolation (10) preserves the self-adjoint symmetry of heterogeneous systems in the form (3).*

2.3.1 Accuracy of Lagrangian patch coupling

For Lagrangian coupling order $\mathbf{P} \geq 4$ plots of simulations are visually similar to those for spectral coupling such as Figure 4. To investigate the homogenisation accuracy of the patch scheme with Lagrangian coupling, we compute the eigenvalues of the microscale heterogeneous matrix operator \mathcal{L} in (4) and compare them to eigenvalues obtained from spectral coupling (Section 2.2) with otherwise identical parameters.

The modes which dominate the emergent homogenised dynamics are those corresponding to the smallest magnitude eigenvalues. The heterogeneous diffusion system (2) has nonpositive eigenvalues of approximately $-k^2$ for wavenumbers $k = 0, 1, 2, \dots$ in our scenarios. For \mathbf{N} patches a patch dynamics simulation supports \mathbf{N} ‘macroscale’ eigen-modes, those with eigenvalues of small magnitude. The remaining eigenvalues are of large magnitude, and represent rapidly decaying sub-patch modes that are of negligible interest. Generally, there is a large gap between the microscale and macroscale eigenvalues, typically $\propto 1/r^2$. In the scenarios reported here, typically the ratio between the large magnitude microscale eigenvalues and the small magnitude macroscale eigenvalues is of the order of 100. So our focus here is assessing

Figure 6: Log-log plot of relative errors of the first five unique nonzero macroscale eigenvalues of \mathcal{L} in (4) with coupling order $P = 5$, domain size 2π , and the period five diffusion coefficients of Figure 4, but different numbers of patches N and patch sizes n while keeping the same microscale spacing $d = rH/n$ for all data. The reference eigenvalues to the right are from spectral coupling with $r = 0.1$. The markers $\circ, \times, +$ correspond to patch size ratios $r = 0.1, 0.4, 0.8$, respectively, and the solid lines join $r = 0.1$ data. Dashed grey lines display the power law N^{-10} , that is, H^{10} .



the accuracy of the first few smallest magnitude eigenvalues compared to the homogenised dynamics.

For a given order P of interpolation, the main factor determining the accuracy of the computational homogenised simulation is the macroscale H which defines the inter-patch spacing. As in classic numerical considerations, the reason is simply that closer spacing better interpolates the *macroscale* structures. We explore a domain of fixed length 2π so that the inter-patch spacing H decreases as the number of patches N increases. Figure 6 illustrates that as the spacing decreases the patch scheme more accurately determines the lowest magnitude nonzero macroscale eigenvalues. We do not show errors

for the zero eigenvalue because this eigenvalue is always calculated to have magnitude no more than 10^{-9} , which is essentially zero (to round-off error). For the non-zero eigenvalues, [Figure 6](#) shows that their error decreases as the power-law $\sim H^{10} \propto N^{-10}$ as expected for the eleven patch stencil width of the coupling order $P = 5$.

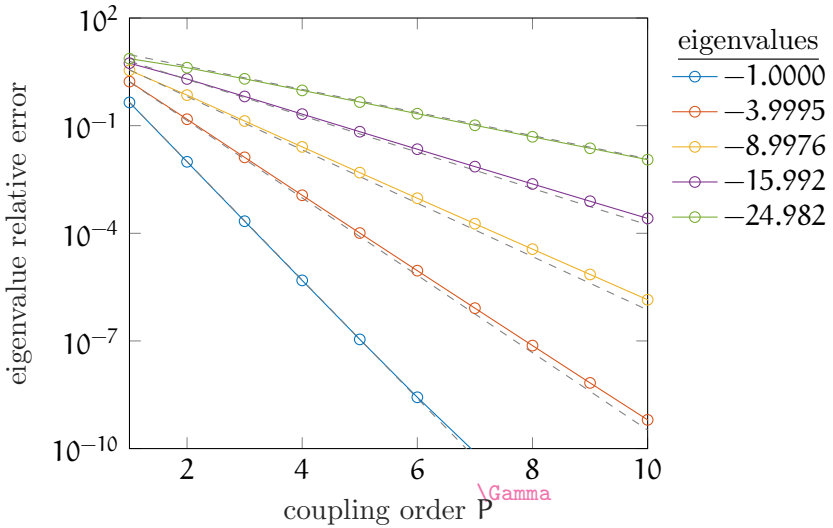
The solid lines of [Figure 6](#) highlight the data at fixed patch size ratio $r = 0.1$. That is, as the inter-patch spacing is decreased, the patch size is proportionally decreased. The microscale lattice spacing d is fixed for all of [Figure 6](#), so the underlying heterogeneous microscale system is the same for all data in the figure. The figure also plots errors for other patch size ratios $r = 0.4, 0.8$, and this data verifies that the errors in the patch scheme have only a weak dependence upon the patch size. That is, for computational efficiency, choose as small a patch as necessary to resolve the microscale dynamics.

In application to some large-scale physical scenario we would require the patch scheme to resolve spatial structures on some macroscale, and so you choose the inter-patch spacing H accordingly. For a given domain this determines the number of patches. Then choose an inter-patch coupling order P , for the Lagrangian spatial coupling (10), to suit your desired error in predictions by the patch scheme. [Figure 7](#) demonstrates that the errors for the macroscale modes of the patch scheme decrease exponentially quickly in the order P of inter-patch coupling. The lessened rate of the exponential decrease for higher wavenumbers, here error $\propto \exp[-\alpha(2 - \log k)P]$, is due to the smaller scale macroscale modes having fewer patches to resolve their structure. [Figure 7](#) is for $N = 20$ patches with size ratio $r = 0.1$, but other parameter choices produce much the same plot: in the computational homogenisation of the patch scheme, relative errors generally decrease exponentially with the order P of Lagrangian inter-patch coupling.

2.4 An ensemble removes periodicity limitation

[Section 2.1](#) deduced that this new patch scheme preserves a self-adjoint heterogeneous system when the size n of the patch is an integral multiple of the diffusivity period p . This section proves that by using an ensemble

Figure 7: Relative errors of the first five nonzero macroscale eigenvalues obtained from different widths of inter-patch coupling. Here the errors are for $N = 20$ patches on a domain of 2π , with patch size $n = 5$, and patch size ratio $r = 0.1$. The dashed grey lines approximate the data by error $\approx 20k^{\alpha P} e^{-2\alpha P}$ for constant $\alpha = 1.9$ and wavenumber $k = 1 : 5$. Spectral coupling gives the reference eigenvalues list in the right-hand column. The diffusion coefficients $\kappa_{i+1/2}$, with period five, are the same as those of Figure 4.



of phase-shifts of the diffusivities, the patch scheme can still preserve self-adjoint symmetry *without* requiring the integral multiple limitation. As long recognised in Statistical Mechanics, a rigorous route to modelling is by considering an ensemble (e.g. van Kampen 1992; Sethna 2006).

We consider an ensemble with \mathbf{p} -members of the heterogeneous system (2) with each member of the ensemble distinguished by a different phase shift of the \mathbf{p} -periodic diffusivities $\kappa_{i+1/2}$. Importantly, do not think of this as an ensemble of a patch scheme for (2), but instead think of it as a patch scheme applied to an ensemble of (2). In multiscale modelling ensembles constructed from microscale phase shifts are useful in many different contexts; for example, Runborg, Theodoropoulos, and Kevrekidis (2002) applied projective integration in a coarse bifurcation analysis of an evolution equation with spatially varying coefficients, with an ensemble constructed from phase shifts in *time*, in contrast to the spatial phase shifts considered here.

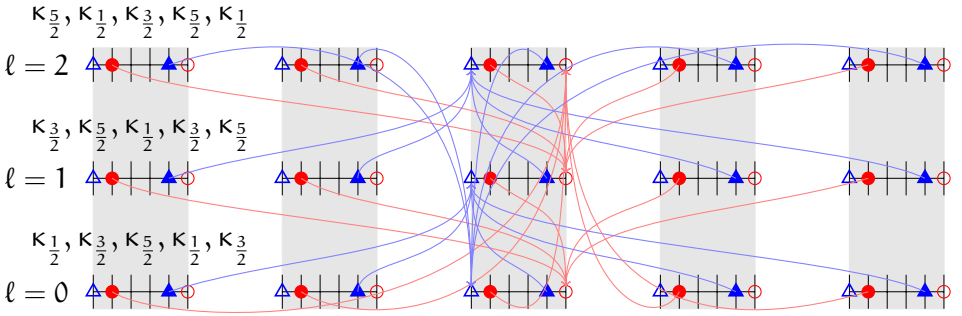
To form the ensemble let $\mathbf{u}_{i,\ell}(\mathbf{t})$ be the field value at location \mathbf{x}_i in the ℓ th member of the ensemble, for $\ell = 0 : \mathbf{p} - 1$. These satisfy all phase-shifts of the diffusivities in the ODEs (2), namely

$$\mathbf{d}^2 \partial_{\mathbf{t}} \mathbf{u}_{i,\ell} = \kappa_{i+\ell+1/2} (\mathbf{u}_{i+1,\ell} - \mathbf{u}_{i,\ell}) + \kappa_{i+\ell-1/2} (\mathbf{u}_{i-1,\ell} - \mathbf{u}_{i,\ell}). \quad (11)$$

Throughout, the diffusivity subscripts are to be interpreted modulo their periodicity \mathbf{p} . Form patches of this ensemble-system as in Figure 2 with $\mathbf{u}_{i,\ell}^I(\mathbf{t})$ denoting the evolving field values in the I th patch at spatial location \mathbf{x}_i^I . Figure 8 illustrates five patches in the case of an ensemble of three members for patches of size $\mathbf{n} = 4$ of a system with diffusivity period $\mathbf{p} = 3$.

Figure 8 illustrates the proposed interpolation of edge values from next-to-edge values in the ensemble, and shows a tangle of dependencies. This inter-patch communication arises in the following way based upon the analysis and notation of the previous Sections 2.1 to 2.3. The previous symbol \mathbf{u}_i^I here denotes the ensemble vector $(\mathbf{u}_{i,0}^I, \dots, \mathbf{u}_{i,\mathbf{p}-1}^I) \in \mathbb{R}^{\mathbf{P}}$. The previous diffusivity $\kappa_{i\pm 1/2}^I$ is here to denote the diffusivity matrix $\text{diag}(\kappa_{i\pm 1/2}, \dots, \kappa_{i+\mathbf{p}-1\pm 1/2}) \in \mathbb{R}^{\mathbf{P} \times \mathbf{P}}$ (subscripts modulo \mathbf{p} as always). Then the patch scheme applied to the heterogeneous ensemble (11) is symbolically the ODEs (3) but here interpreted as matrix-vector ODEs instead

Figure 8: Five patches of the three member ensemble of phase-shifts in the case of diffusivity period $p = 3$ and $n = 4$ patch interior points: the diffusivities are $\kappa_{1/2}, \kappa_{3/2}, \kappa_{5/2}$. Lattice points and patches in the same column are at the same physical location. For the middle patch in each member, u -values at the edges $i = 0, 5$ (unfilled triangles/circles) are interpolated from u -values of next-to-edge points $i = 4, 1$ (filled triangles/circles) in neighbouring patches, but from a different member in order to preserve self-adjoint symmetry.

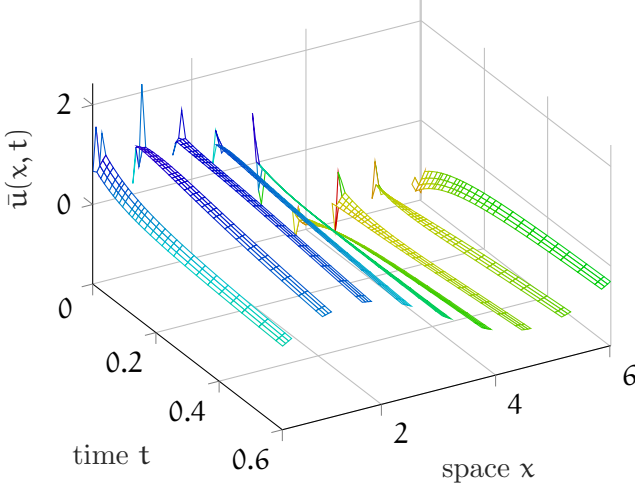


of scalar ODEs.

Consequently, all the arguments and results of the previous Sections 2.1 to 2.3 apply here also. Except that we now have extra freedom in the patch-coupling interpolation matrix. Previously the symbol \mathcal{C}_{ij}^{IJ} was a scalar, but here represents a $p \times p$ block in the ensemble system's $nNp \times nNp$ matrix. Thus we have the freedom to choose the crucial interpolation blocks $\mathcal{C}_{n1}^{IJ}, \mathcal{C}_{1n}^{IJ}$ in non-diagonal form. The tangle of inter-patch communication in Figure 8 represents a non-diagonal $\mathcal{C}_{n1}^{IJ}, \mathcal{C}_{1n}^{IJ}$.

We choose $\mathcal{C}_{n1}^{IJ}, \mathcal{C}_{1n}^{IJ}$ to preserve self-adjoint symmetry, and Assumption A1 and Assumption A2. In the l th member of the ensemble, the l th row of Figure 8, has diffusivity $\kappa_{n+l+1/2}$ (subscript mod p) at the right-edge of patches. So the interpolation from its right-next-to-edges is chosen to determine the left-edge values of member $(n + l \text{ mod } p)$ because it has the same diffusivity $\kappa_{n+l+1/2}$ at its left-edge. Correspondingly in reverse for

Figure 9: the ensemble-mean field $\bar{u}(x, t)$ in a simulation of an ensemble of heterogeneous diffusion (11) on nine patches with spectral coupling (8) and patch-ratio $r = 0.3$, for comparison with Figure 4. The diffusion coefficients $\kappa_{i+1/2}$ with period $p = 5$ are as in Figure 4, but here there are just $n = 4$ patch interior points, as plotted.



interpolation from left-next-to-edges to right-edge values. Hence, setting the $p \times p$ matrix K to zero except for $K_{\ell+1, (\ell+n \bmod p)+1} := \kappa_{\ell+1/2}$, $\ell = 0 : p - 1$, let's choose

$$\mathcal{C}_{1n}^{IJ} := K \mathcal{I}_{1n}^{IJ} \quad \text{and} \quad \mathcal{C}_{n1}^{IJ} := K^\dagger \mathcal{I}_{n1}^{IJ} \quad (12)$$

in terms of the scalar interpolation coefficients \mathcal{I}_{ij}^{IJ} of the interpolation schemes of Sections 2.2 and 2.3. Because of this choice of K , the above argument establishes the following lemma.

Lemma 4. *The inter-patch coupling with (12) preserves self-adjoint symmetry in the ensemble of heterogeneous diffusion systems (11).*

As an example, Figure 9 plots a simulation of our patch scheme applied to heterogeneous diffusion with diffusivity period $p = 5$ and the same diffusion coefficients as listed in Figure 4. With the exception of the number of patch interior

points, which here is $n = 4$, the parameters of Figure 9 are the same as in Figure 4. At each spatial point x_i^I there are five ensemble values $u_{i,0}^I, \dots, u_{i,4}^I$ so Figure 9 plots the ensemble-mean $\bar{u}(x_i^I, t) := \frac{1}{p} \sum_{\ell=0}^{p-1} u_{i,\ell}^I(t)$. In the simulation of Figure 9, all five members of the ensemble were given the same initial condition, and this initial condition is the same as that for Figure 4 but with a different random component. Because of the average over the ensemble, Figure 9 does not exhibit the rough microscale structure shown in Figure 4 that arises from just one phase of the heterogeneous diffusivity.

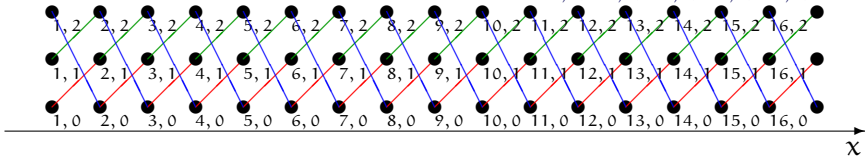
To verify the accuracy of the patch scheme applied to the ensemble of phase-shifts, we investigated the accuracy of the small-magnitude eigenvalues that correspond to the macroscale modes in the computational scheme. Over a range of coupling orders P , we plotted the relative errors of nonzero macroscale eigenvalues of ensemble matrix \mathcal{L} for Lagrangian spatial coupling (10) (relative to the spectral eigenvalues (8)). The plots were graphically indistinguishable from that of Figure 7—so are not reproduced here. The crucial difference is that here we used an ensemble of patches of size $n = 4$ points—a size which is not an integral multiple of the diffusivity period $p = 5$. Evidently the patch scheme applied to an ensemble for general patch size of n points appears to be just as accurate as for the well-known special case of n being an integral multiple of the period p . Section 3 establishes this accuracy in general.

Invoking this ensemble of all phase-shifts of the diffusivities allows any size patch, any n , while appearing to maintain the full accuracy of the computational homogenisation supplied by the patch scheme, albeit with an increase in the computation. We conjecture that if the heterogeneous diffusivities is random, with no period, then an ensemble of realisations will provide more accurate predictions than a single realisation.

3 The patch scheme is consistent to high-order

This section develops theoretical support for the accuracy of the patch scheme with self-adjoint coupling. But before we discuss patches, we reconsider the heterogeneous diffusion (2) and its ensemble of all phase shifts (11). Section 3.1 establishes that the ensemble system describes the correct macroscale

Figure 10: embed the heterogeneous diffusion (2) into p replications of itself, here for the case $p = 3$. The circles denote values $v_{i,\ell}(t)$ for the example labelled values i, ℓ , and the coloured lines denote the heterogeneous diffusion between $v_{i,\ell}$ that both replicates (2), but is now spatially homogeneous, in x , on the lattice. Over x , the fields $v_{i,\ell}(t)$ of any one of the $p = 3$ phases follow the coloured diagonals representing the heterogeneous diffusion for that phase, for example, one phase has fields $v_{1,1}, v_{2,2}, v_{3,3}, v_{4,1}, v_{5,2}, \dots$



homogenised behaviour. Section 3.2 then proves that the patch scheme with self-adjoint coupling of the ensemble is consistent with the ensemble system, and hence with the heterogeneous diffusion (2).

In this and the next section, the term “consistent” means “consistent with arbitrarily high-order in H ”, unless otherwise specified.

We use consistency to assess accuracy of the patch scheme because the usual numerical analysis, of the finite element and finite volume methods, involves integrals over space which in a patch scheme would be integrals over much uncomputed space and so appear to be inappropriate for a patch scheme.

Section 2.4 creates the ensemble of phase shifts by directly ‘stacking vertically’ each member in the ensemble, as illustrated by Figure 8. This appears best for computation. Best because a user codes the lattice dynamics in the ‘horizontal’ direction as usual, and then the tangle of inter-patch communication (Figure 8) may be managed by a generic patch function as in our toolbox (Roberts, Maclean, and Bunder 2020).

However, for theoretical analysis it appears best, and we take this route here, to form the ensemble so that each member of the ensemble is ‘wrapped diagonally’, as illustrated by Figure 10 for the case of periodicity $p = 3$. In terms of $u_{i,\ell}$ of Section 2.4, define $v_{i,\ell}(t) := u_{i,(i-\ell \bmod p)}$. That is, $v_{i,\ell}$ is a field value at position x_i , for $\ell = 0 : p - 1$, and $\phi = i - \ell \bmod p$ identifies

the physical phase-shift for the member of the ensemble. According to (11) these evolve in time according to the ODEs

$$d^2 \partial_t v_{i,\ell} = \kappa_{\ell+1/2}(v_{i+1,\ell+1} - v_{i,\ell}) + \kappa_{\ell-1/2}(v_{i-1,\ell-1} - v_{i,\ell}), \quad (13)$$

where we adopt the convention that both the subscript of κ and the second subscript of v is always interpreted modulo the microscale periodicity p . Consequently, $u_i(t) := v_{i,i+\phi}$ then satisfies the original diffusion (2), but with the diffusivities phase shifted by ϕ . That is, the system (13) for $v_{i,\ell}$ captures the p microscale-phase shifted versions (11) of the original heterogeneous diffusion (2). As in macroscale modelling (Roberts 2015a, §2.5), the big advantage of (13) is that the heterogeneity only occurs in ℓ and is independent of, *homogeneous* in, the spatial index i . This homogeneity is unlike systems (2) and (11) where the heterogeneity explicitly varies with the spatial index. The homogeneity of (13) in spatial index i is crucial in developing theory.

3.1 An ensemble has the correct homogenisation

The aim of this subsection is to establish that the solutions of the ensemble system (13) track solutions of an effective ‘homogenised’ PDE $V_t = \mathcal{K}_2 V_{xx}$ for a field $V(x, t)$ and an effective diffusivity \mathcal{K}_2 .

We analyse the long-time dynamics via the Fourier transform in space (Roberts 2015b, §7.2 and Exercise 7.5). For grid-scaled spatial Fourier wavenumber k we seek solutions $v_{i,\ell}(t) = \int_{-\pi}^{\pi} e^{ik_i} \tilde{v}_\ell(k, t) dk$ (for $i := \sqrt{-1}$, distinct from lattice index i). Because of the linear independence of e^{ik_i} , (13) becomes, for every wavenumber k ,

$$d^2 \partial_t \tilde{v}_\ell = \kappa_{\ell+1/2}(e^{ik} \tilde{v}_{\ell+1} - \tilde{v}_\ell) + \kappa_{\ell-1/2}(e^{-ik} \tilde{v}_{\ell-1} - \tilde{v}_\ell), \quad \ell = 0 : p - 1. \quad (14)$$

This system has a subspace of equilibria for wavenumber $k = 0$ and $\tilde{v}_\ell = \text{constant}$. Since the problem is linear in \tilde{v} , without loss of generality we analyse the case of equilibrium $\tilde{v}_\ell = 0$ (Roberts 2015b, §7.2). When wavenumber $k = 0$ the system (14) has one eigenvalue of zero, and $(p - 1)$ negative eigenvalues $\lambda \leq -\beta$ for bound $\beta = 2\pi^2 \min_\ell \kappa_{\ell+1/2}/(p^2 d^2)$. Notionally adjoining $dk/dt =$

0, we deduce there exists an emergent slow manifold of (14) for a range of small \mathbf{k} , and globally in $\tilde{\mathbf{v}}$ (Carr 1981).

Straightforward construction (Roberts 2015b, as in Exercise 7.5) leads to the evolution on the slow manifold, in terms of some chosen parameter $\tilde{\mathbf{V}}(\mathbf{k}, \mathbf{t})$. Here we describe the evolution on the slow manifold in terms of the mean Fourier component $\tilde{\mathbf{V}}(\mathbf{k}, \mathbf{t}) := \frac{1}{\mathbf{p}} \sum_{\ell} \tilde{\mathbf{v}}_{\ell}(\mathbf{t})$. We seek the evolution of $\tilde{\mathbf{V}}$ in terms of a power series in small wavenumber \mathbf{k} , up to some specified order. For given diffusivities and periodicity \mathbf{p} , the computer algebra in Appendix A efficiently derives the evolution via an iteration, based upon the residual of (14), from the initial approximation that $\partial_{\mathbf{t}} \tilde{\mathbf{V}} \approx 0$ and $\tilde{\mathbf{v}}_{\ell} \approx \tilde{\mathbf{V}}$ for every $\ell = 0 : \mathbf{p} - 1$. Subsequent iterations provide corrections in terms of $\tilde{\mathbf{V}}$ and powers of \mathbf{k} . In general, the dynamical evolution on the slow manifold is then of the form

$$\mathbf{d}^2 \partial_{\mathbf{t}} \tilde{\mathbf{V}} = -\mathbf{k}^2 \mathcal{K}_2 \tilde{\mathbf{V}} + \mathbf{k}^4 \mathcal{K}_4 \tilde{\mathbf{V}} + \dots, \quad (15)$$

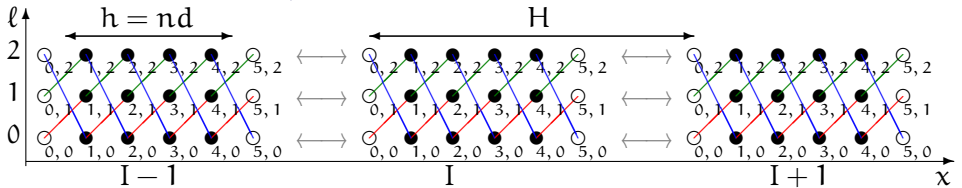
for $\mathcal{K}_2 := \mathbf{n} / (\sum_{\ell} \kappa_{\ell+1/2}^{-1})$, and some complicated \mathcal{K}_4 . As an example, for periodicity $\mathbf{p} = 3$ and $\kappa_{\ell+1/2} = \ell + 1$; Appendix A computes $\mathcal{K}_2 = \frac{18}{11}$ and $\mathcal{K}_4 = \frac{675}{2662}$.

We obtain a physical space PDE for the macroscale by integrating over small wavenumbers (Roberts 2015b, Exercise 7.5). Let \mathbf{k}_c denote a cut-off wavenumber, suitable to capture the macroscales of interest, and define $\mathbf{V}(\mathbf{x}, \mathbf{t}) := \int_{-\mathbf{k}_c}^{\mathbf{k}_c} e^{i\mathbf{k}\mathbf{x}/\mathbf{d}} \tilde{\mathbf{V}}(\mathbf{k}, \mathbf{t}) \mathbf{d}\mathbf{k}$. Upon correspondingly integrating (15), we deduce the emergent slow manifold dynamics is equivalently governed by the ‘homogenised’ PDE

$$\frac{\partial \mathbf{V}}{\partial \mathbf{t}} = \mathcal{K}_2 \frac{\partial^2 \mathbf{V}}{\partial \mathbf{x}^2} + \mathcal{K}_4 \mathbf{d}^2 \frac{\partial^4 \mathbf{V}}{\partial \mathbf{x}^4} + \dots. \quad (16)$$

The coefficient $\mathbf{d}^2 \mathcal{K}_4$ indicates that our approach supports not only the classic diffusion homogenisation as the microscale $\mathbf{d} \rightarrow 0$, but also establishes corrections at finite \mathbf{d} . Such higher-order corrections are needed in some homogenisation applications (e.g., Cornaggia and Guzina 2020). We also contend that the technique of Roberts (2015a) would extend to provide, at finite scale separation \mathbf{d} , a rigorous error formula for any finite truncation of this asymptotic series, and would also do so for nonlinear systems.

Figure 11: example of patch scheme (Figure 2) with $n = 4$ points in each patch, for an ensemble with heterogeneity of period $p = 3$ (Figure 10). These homogeneous patches are coupled, as in Figure 3, by interpolation to the left/right edge of a patch from the next-to-edge points on the right/left of nearby patches and always to points with the same ℓ . For each $\ell = 0 : p - 1$, the value $v_{5,\ell}^I$ is interpolated from values $v_{1,\ell}^J$ from nearby patches J , and $v_{0,\ell}^I$ is interpolated from $v_{4,\ell}^J$.



This approach rigorously establishes that the classic homogenisation of the ensemble system (13) is the leading approximation to the evolution of long wavelength structures on the lattice. Moreover, the centre manifold emergence theorem (e.g., Roberts 2015b, §4.3) assures us that all solutions approach this homogenisation on a cross-period diffusion time $\propto 1/\beta$.

3.2 High-order consistency of the patch scheme

This section establishes that when the phase-shifted ensemble system (13) (Figure 10) is restricted to patches, with self-adjoint coupling as in Figure 11, the resulting patch system maintains consistency with (13). The analysis shows that any errors arising in the scheme are due to the choice of coupling condition. The advantage of the ensemble (13) for the patch scheme is that the microscale system within patches is homogeneous in the x -index i ; the heterogeneity in the original diffusion (2) only appears here in the cross-section indexed by ℓ (Figure 11).

Corresponding to Section 2, let the macroscale spacing in x of the patches be H —much larger than the microscale lattice spacing d . Let the patches have n interior points so the patches are of width $h := nd$ in x , and let the ratio $r := h/H$. Also let $v_{i,\ell}^I(t)$ to denote the field value at the (i, ℓ) th point

Table 1: Useful operator identities based upon the shift E which shifts an operand to the right by some ‘distance’ Δ (Natl Physical Lab 1961, p65, e.g.). A subscript on any of the listed operators defines the distance Δ . For example, E_i increases the index i by one (distance $\Delta = d$), and E_x increases the position x by H (distance $\Delta = H$).

$E u(x) := u(x + \Delta)$	$E^{\pm 1} = 1 \pm \mu \delta + \frac{1}{2} \delta^2$
$\delta := E^{1/2} - E^{-1/2}$	$\mu := \frac{1}{2}(E^{1/2} + E^{-1/2})$
$\delta = 2 \sinh(\Delta \partial_x / 2)$	$\mu = \cosh(\Delta \partial_x / 2)$
$\Delta \partial_x = 2 \operatorname{asinh}(\delta / 2)$	$\mu^2 = 1 + \frac{1}{4} \delta^2$

of the lattice within the I th patch (Figure 11). For generality, let the vector $\mathbf{v}(t) \in \mathbb{R}^p$ denote the vector of p values at each x , and then for patches the vector $\mathbf{v}_i^I := (v_{i,0}^I, \dots, v_{i,p-1}^I)$. That is, here the vector \mathbf{v} corresponds to the scalar u of Section 2. We now use shift, difference, and mean operators as defined by Table 1 to express and analyse this patch scheme for the ensemble.

Lemma 5. *The ensemble system (13) is of the vector form*

$$\partial_t \mathbf{v}_i = \delta_i (\hat{K} E_i^{1/2} - \check{K} E_i^{-1/2}) \mathbf{v}_i + D \mathbf{v}_i, \quad i = 1 : n, \quad (17)$$

for the three $p \times p$ matrices D , \hat{K} and \check{K} .

Proof. Let’s rewrite the ensemble lattice ODES (13) for patch interior indices $i = 1 : n$:

$$\begin{aligned} d^2 \partial_t v_{i,\ell} &= \kappa_{\ell+1/2} (v_{i+1,\ell+1} - v_{i,\ell+1}) + \kappa_{\ell-1/2} (v_{i-1,\ell-1} - v_{i,\ell-1}) \\ &\quad + \kappa_{\ell+1/2} (v_{i,\ell+1} - v_{i,\ell}) + \kappa_{\ell-1/2} (v_{i,\ell-1} - v_{i,\ell}) \\ &= \delta_i (\kappa_{\ell+1/2} v_{i+1/2,\ell+1} - \kappa_{\ell-1/2} v_{i-1/2,\ell-1}) + \delta_\ell (\kappa_\ell \delta_\ell v_{i,\ell}) \\ &= \delta_i (\kappa_{\ell+1/2} E_i^{1/2} v_{i,\ell+1} - \kappa_{\ell-1/2} E_i^{-1/2} v_{i,\ell-1}) + \delta_\ell (\kappa_\ell \delta_\ell v_{i,\ell}), \end{aligned}$$

on applying operator definitions given in Table 1. Define the cell-diffusion $p \times p$ matrix D to encode the operator $\delta_\ell (\kappa_\ell \delta_\ell \cdot) / d^2$, and the shifted-diffusivity $p \times p$ matrix K to be zero except $K_{i,i+1} := \kappa_{i+1/2} / d^2$ for $i = 1 : p - 1$ and

$K_{p,1} := \kappa_{1/2}/d^2$. Then the above ODEs become the vector system (17) with matrices $\hat{K} := K$ and $\check{K} := K^\top$. \square

Since Lemma 5 establishes that (13) and (17) are the same, we propose a patch scheme for the heterogeneous diffusion system (13) of the form

$$\text{solve (17) for } \mathbf{v}_i^I \text{ instead of } \mathbf{v}_i, \text{ with } \mathbf{v}_{n+1}^I = E_x^r \mathbf{v}_1^I, \quad \mathbf{v}_0^I = E_x^{-r} \mathbf{v}_n^I, \quad (18)$$

as the inter-patch coupling via the edge-values. In the inter-patch coupling of (18), since the shift E_x describes a macroscale shift of H , the shift E_x^r describes a macroscale fractional shift of $rH = nd$; that is, E_x^r describes a shift over the width of a patch. So $E_x^r \mathbf{v}_1^I$ shifts each element from the left-next-to-edge point to the corresponding element on the right edge \mathbf{v}_n^I , and similarly, $E_x^{-r} \mathbf{v}_n^I$ shifts from the right-next-to-edge value to the left edge \mathbf{v}_0^I . The following Theorem 6 justifies the patch scheme (18).

Theorem 6. *The macroscale of the patch scheme (18) is consistent with the microscale dynamics of (17) over the entire spatial domain, and hence with the ensemble (13).*

This theorem may appear almost vacuous as the ODEs (17) are common to both parts of the claim. However, the distinction is that the ‘‘patch scheme (18)’’ has the ODEs (17) holding only inside small, well-separated, patches of the spatial domain, whereas the ‘‘dynamics of (17)’’ are to hold on a lattice over the entire spatial domain. With very different domains, they are two very different dynamical systems, and so the following proof is deeper than may be first appear necessary.

Proof of Theorem 6. Consider the vector system (17) on patches coupled by the interpolation (18). Using Table 1, the system

$$\begin{aligned} \partial_t \mathbf{v}_i^I &= \delta_i (\hat{K} E_i^{1/2} - \check{K} E_i^{-1/2}) \mathbf{v}_i^I + D \mathbf{v}_i^I \\ \iff \partial_t \mathbf{v}_i^I - D \mathbf{v}_i^I &= 2 \sinh[d \partial_x / 2] (\hat{K} E_i^{1/2} - \check{K} E_i^{-1/2}) \mathbf{v}_i^I \\ \iff (\partial_t - D) \mathbf{v}_i^I &= 2 \sinh\left[\frac{1}{n} \operatorname{asinh}(\bar{\delta}/2)\right] (\hat{K} E_i^{1/2} - \check{K} E_i^{-1/2}) \mathbf{v}_i^I \end{aligned}$$

for centred difference $\bar{\delta} := E_i^{n/2} - E_i^{-n/2} = 2 \sinh(\mathbf{n}d\partial_x/2)$, as the difference is over a distance $\Delta = \mathbf{h} = \mathbf{n}d$. Invoking cognate steps to those of the proof by Roberts, MacKenzie, and Bunder (2014), let's invert the operator function $f(\bar{\delta}) := 2 \sinh[\frac{1}{n} \operatorname{asinh}(\bar{\delta}/2)]$ and write the above dynamical equation as

$$\begin{aligned} & f^{-1}(\partial_t - D)\mathbf{v}_i^I \\ &= \bar{\delta}(\hat{K}E_i^{1/2} - \check{K}E_i^{-1/2})\mathbf{v}_i^I \\ &= E_i^{n/2}(\hat{K}E_i^{1/2} - \check{K}E_i^{-1/2})\mathbf{v}_i^I - E_i^{-n/2}(\hat{K}E_i^{1/2} - \check{K}E_i^{-1/2})\mathbf{v}_i^I \\ &= \hat{K}\mathbf{v}_{i+n/2+1/2}^I - \check{K}\mathbf{v}_{i+n/2-1/2}^I - \hat{K}\mathbf{v}_{i-n/2+1/2}^I + \check{K}\mathbf{v}_{i-n/2-1/2}^I. \end{aligned}$$

Now evaluate this equation at the patch mid-point, $i = n/2 + 1/2$ (a virtual mid-point when size n is even), and here define the macroscale $\mathbf{V}^I(\mathbf{t}) := \mathbf{v}_{n/2+1/2}^I \in \mathbb{R}^P$. Hence

$$\begin{aligned} & f^{-1}(\partial_t - D)\mathbf{V}^I \\ &= \hat{K}\mathbf{v}_{n+1}^I - \check{K}\mathbf{v}_n^I - \hat{K}\mathbf{v}_1^I + \check{K}\mathbf{v}_0^I \\ &= \hat{K}E_x^r\mathbf{v}_1^I - \check{K}\mathbf{v}_n^I - \hat{K}\mathbf{v}_1^I + \check{K}E_x^{-r}\mathbf{v}_n^I \quad (\text{by edge interpolation}) \\ &= \hat{K}(E_x^r - 1)\mathbf{v}_1^I - \check{K}(1 - E_x^{-r})\mathbf{v}_n^I \\ &= (E_x^{r/2} - E_x^{-r/2})(\hat{K}E_x^{r/2}\mathbf{v}_1^I - \check{K}E_x^{-r/2}\mathbf{v}_n^I) \quad (\text{by commutativity}). \end{aligned}$$

The above right-hand side is on the macroscale because it involves the macroscale inter-patch interpolation via the operator E_x . To compare with the original system, we transform this macroscale identity back to its equivalent on the microscale lattice. To do so, notionally evaluate over the microscale the smooth macroscale interpolation underlying the operators $E_x^{\pm r/2}$ so that for the interpolated field we have $E_x^{\pm r/2} = E_i^{\pm n/2}$. Hence, for the smooth macroscale field from the patch scheme, the above identity becomes

$$\begin{aligned} & f^{-1}(\partial_t - D)\mathbf{V}^I \\ &= (E_i^{n/2} - E_i^{-n/2})(\hat{K}E_i^{n/2}\mathbf{v}_1^I - \check{K}E_i^{-n/2}\mathbf{v}_n^I) \\ &= \bar{\delta}(\hat{K}\mathbf{v}_{n/2+1}^I - \check{K}\mathbf{v}_{n/2}^I) = \bar{\delta}(\hat{K}E_i^{1/2} - \check{K}E_i^{-1/2})\mathbf{v}_{n/2+1/2}^I \\ &= \bar{\delta}(\hat{K}E_i^{1/2} - \check{K}E_i^{-1/2})\mathbf{V}^I. \end{aligned}$$

Now revert the function f^{-1} , recalling $f(\bar{\delta}) = \delta_i$, to deduce that

$$\begin{aligned} (\partial_t - D)\mathbf{V}^I &= f(\bar{\delta})[(\hat{\mathcal{K}}\mathcal{E}_i^{1/2} - \check{\mathcal{K}}\mathcal{E}_i^{-1/2})\mathbf{V}^I] \\ \iff \partial_t\mathbf{V}^I &= \delta_i[(\hat{\mathcal{K}}\mathcal{E}_i^{1/2} - \check{\mathcal{K}}\mathcal{E}_i^{-1/2})\mathbf{V}^I] + D\mathbf{V}^I. \end{aligned} \quad (19)$$

The operator on the right-hand side is precisely the same as that for the microscale. Thus, in this patch scheme, the evolution over the macroscale of the mid-patch values \mathbf{V}^I are consistent with the microscale evolution (17). \square

Consequently, any errors in the macroscale of this patch scheme applied to (13) arise only from errors in the interpolation of the edge values (and the usual round-off errors).

Corollary 7. *The patch scheme (18) (or Section 2.4) applied to the ensemble (13) of the heterogeneous diffusion (2), is consistent with the homogenisation (16) of the heterogeneous diffusion (2).*

Proof. Recall that (13) is an ensemble of \mathfrak{p} uncoupled, phase-shifted, copies of the heterogeneous diffusion (2). So the results for (13) apply to (2). Also, the centre manifold theory supported homogenisation (16) is a ‘PDE’ of a superposition, a linear combination, a low-pass filter, of exact solutions of the ensemble (13), and hence of (2). Theorem 6 proves the patch scheme (18) is consistent with the ensemble (13), and so it is consistent with the homogenisation (16) of the heterogeneous diffusion (2). \square

Corollary 8. *If the chosen size \mathfrak{n} of the patches is a multiple of the microscale periodicity \mathfrak{p} , then the patch scheme applied directly to the heterogeneous diffusion (2) (without the ensemble of phase shifts) is consistent with the homogenisation of (2).*

Proof. Recall that, among the ensemble of phase-shifted diffusivities, $v_{i,\ell}^I$ is the member with phase $\phi = (i - \ell \bmod \mathfrak{p})$. Further recall that coupling is always between edge fields and next-to-edge fields with the same ℓ value, so that $v_{0,\ell}^I$ is computed from interpolations of $v_{\mathfrak{n},\ell}^J$, and $v_{\mathfrak{n}+1,\ell}^I$ is computed from interpolations of $v_{1,\ell}^J$, for some patches J neighbouring patch I . For most \mathfrak{n} the inter-patch coupling (18) couples patches via different phases.

For example, Figures 8 and 11 with $n = 4$ and periodicity $p = 3$ couples the right-edge field of phase $\phi = 0$ ($i = 5, \ell = 2$) to the left-next-to-edge fields of $\phi = 2$ ($i = 1, \ell = 2$) in neighbouring patches, and the left-edge field of phase $\phi = 0$ ($i = 0, \ell = 0$) to the right-next-to-edge fields of $\phi = 1$ ($i = 4, \ell = 0$) in neighbouring patches. In general, the inter-patch coupling (18) for $\ell = 0 : p - 1$ has phase ϕ on the right-edge of patch I coupled with phase $\phi - n \bmod p$ left-next-to-edge fields in neighbouring patches, and on the left-edge of patch I coupled with phase $\phi + n \bmod p$ in right-next-to-edge fields neighbouring patches. Consequently, in the cases when p divides n the inter-patch coupling (18) always couples with the same phase from every patch. In these cases the p phases do not interact with each other. That is, when p divides n the patch scheme of an ensemble decouples to p independent equivalent patch systems, and so we need only compute one of these p systems to obtain the benefits of the ensemble results. Thus, Corollary 7 assures us that when p divides n the patch scheme applied to the heterogeneous diffusion (2) is consistent with the homogenisation (16) of (2). \square

4 Self-adjoint preserving patch scheme for 2D

Recall that Figure 1 illustrates a patch scheme simulation that provides a computational homogenisation of the heterogeneous 2D diffusion (1) on a microscale lattice. We explore the patch scheme applied to (1) as it is the canonical example of the homogenisation of heterogeneous PDEs in multiple spatial dimensions. We first define how to coupling patches in 2D, confirm that the 2D patch scheme is self-adjoint, and then verify the accuracy when using spectral coupling (Section 4.1). For 2D heterogeneous diffusion (1), patch coupling is constrained in the same way as the 1D heterogeneous diffusion patch coupling; namely that we require the patch size to be divisible by the period of the heterogeneous diffusion; but like the 1D case, an ensemble of phase-shifts relaxes this constraint (Section 4.2). Finally, we prove that the resultant 2D patch scheme is consistent with the macroscale dynamics of the original microscale system (Section 4.3). We conjecture there is a straightforward extension of this patch scheme and theory from 2D to higher

dimensions.

4.1 Self-adjoint coupling for 2D

Consider the 2D heterogeneous diffusion (1). For this 2D case, we create a patch scheme using similar parameters to those defined for the 1D case (e.g., \mathbf{d} , H , N , \mathbf{n} , \mathbf{r}), but now with subscripts \mathbf{x} and \mathbf{y} to distinguish the parameters for the \mathbf{x} and \mathbf{y} directions (Figure 12). The patch scheme divides the 2D domain of this microscale model into well-separated patches on a macroscale lattice indexed by (I, J) with macroscale lattice spacing H_x and H_y , as illustrated by Figures 1 and 12. In the patch scheme, the microscale indices (i, j) index interior points within a patch by $i = 1 : n_x$ and $j = 1 : n_y$. On all such interior points we apply the 2D heterogeneous diffusion (1) but with the patch index specified:

$$\begin{aligned} \partial_t \mathbf{u}_{i,j}^{I,J} = & [\kappa_{i+\frac{1}{2},j}^{I,J} (\mathbf{u}_{i+1,j}^{I,J} - \mathbf{u}_{i,j}^{I,J}) + \kappa_{i-\frac{1}{2},j}^{I,J} (\mathbf{u}_{i-1,j}^{I,J} - \mathbf{u}_{i,j}^{I,J})] / \mathbf{d}_x^2 \\ & + [\kappa_{i,j+\frac{1}{2}}^{I,J} (\mathbf{u}_{i,j+1}^{I,J} - \mathbf{u}_{i,j}^{I,J}) + \kappa_{i,j-\frac{1}{2}}^{I,J} (\mathbf{u}_{i,j-1}^{I,J} - \mathbf{u}_{i,j}^{I,J})] / \mathbf{d}_y^2, \end{aligned} \quad (20a)$$

where the diffusivities have lattice periods p_x and p_y in the \mathbf{x} and \mathbf{y} directions, respectively.

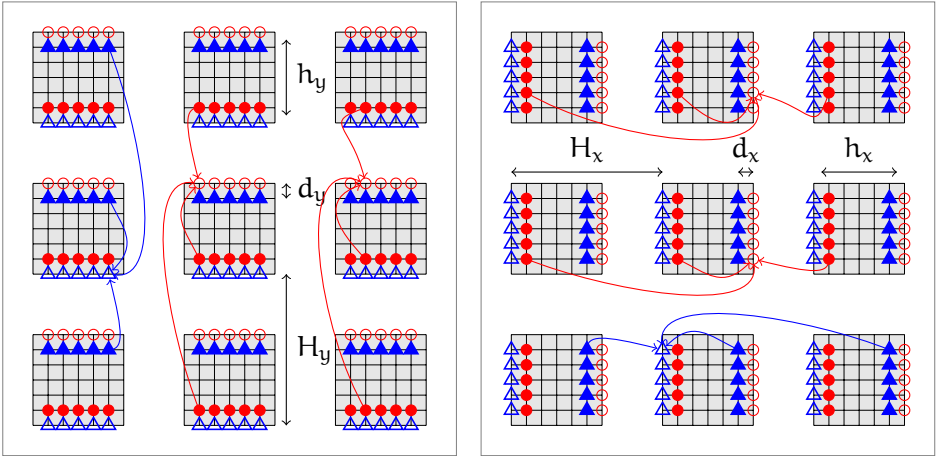
The diffusion equation (20a) requires field values at the edges of every patch, namely $\mathbf{u}_{0,j}^{I,J}$, $\mathbf{u}_{n_x+1,j}^{I,J}$, $\mathbf{u}_{i,0}^{I,J}$ and $\mathbf{u}_{i,n_y+1}^{I,J}$ for $i = 1 : n_x$ and $j = 1 : n_y$. The inter-patch coupling specifies these edge values. Figure 12 illustrates the 2D patch coupling across both \mathbf{x} (to obtain left and right patch-edge values) and \mathbf{y} (to obtain bottom and top patch-edge values). We implement the following 2D form of the 1D coupling (7) in the \mathbf{x} and \mathbf{y} directions, respectively:

$$\mathbf{u}_{0,j}^{I,J} = \sum_K \mathcal{I}_{1n_x}^{IK} \mathbf{u}_{n_x,j}^{K,J} \quad \text{and} \quad \mathbf{u}_{n_x+1,j}^{I,J} = \sum_K \mathcal{I}_{n_x 1}^{IK} \mathbf{u}_{1,j}^{K,J}, \quad j = 1 : n_y; \quad (20b)$$

$$\mathbf{u}_{i,0}^{I,J} = \sum_K \mathcal{J}_{1n_y}^{JK} \mathbf{u}_{i,n_y}^{I,K} \quad \text{and} \quad \mathbf{u}_{i,n_y+1}^{I,J} = \sum_K \mathcal{J}_{n_y 1}^{JK} \mathbf{u}_{i,1}^{I,K}, \quad i = 1 : n_x. \quad (20c)$$

The matrices \mathcal{I} and \mathcal{J} for \mathbf{x} and \mathbf{y} coupling, respectively, are the diffusivity independent matrices of interpolation coefficients and are equivalent to \mathcal{I}

Figure 12: self-adjoint preserving, nearest neighbour ($P = 1$), coupling of patches of size 5×5 : (left) vertical y coupling; and (right) horizontal x coupling. Filled triangles/circles are the next-to-edge points whose values are interpolated to the edge points at unfilled triangles/circles. Interpolation to a bottom/top edge is from the next-to-edge points with the same horizontal position on the top/bottom of the near patches above and below, as indicated by arrows in the left diagram. Similarly for left/right interpolation.



for 1D systems defined in Section 2.1, but depend on different size ratios $r_x = h_x/H_x$ and $r_y = h_y/H_y$, respectively. As in 1D, we choose these coefficients to implement either spectral coupling (Section 2.2), or Lagrangian coupling (Section 2.3).

Figure 1 illustrates a patch simulation of the heterogeneous diffusion (20) for a Gaussian initial condition on a macroscale lattice of 5×5 patches. The patches are of size $n_x = n_y = 3$ in both directions. The 18 microscale diffusion coefficients $\kappa_{i,j}$ have a period of three in both directions and are independently and identically distributed log-normally (proportional to $\exp[2\mathcal{N}(0, 1)]$). The patches are coupled via two sets of 1D spectral interpolation (Section 2.2). From the initially smooth Gaussian, the patch system evolves to a ‘rough’ sub-patch structure that reflects the microscale heterogeneity. Thereafter, the patch system simulates how the field u diffuses across the domain according

to an effective macroscale anisotropic homogenisation.

Figure 13 simulates a similar heterogeneous diffusion but with rectangular patches so that there are geometric differences between the two principal directions. Here the microscale diffusivities are (to two decimal places)

$$\left[\kappa_{i+\frac{1}{2},j} \right] = \begin{bmatrix} 18.91 & 1.06 & 0.63 & 2.11 \\ 4.46 & 0.72 & 1.02 & 1.66 \\ 4.89 & 0.88 & 1.31 & 5.79 \\ 1.62 & 2.68 & 2.32 & 1.24 \\ 0.42 & 0.88 & 0.59 & 1.35 \end{bmatrix}, \quad \left[\kappa_{i,j+\frac{1}{2}} \right] = \begin{bmatrix} 0.48 & 0.63 & 1.31 & 0.51 \\ 0.39 & 10.38 & 3.07 & 0.37 \\ 2.10 & 1.74 & 2.68 & 1.63 \\ 1.20 & 4.38 & 0.50 & 1.02 \\ 2.55 & 1.23 & 0.33 & 1.06 \end{bmatrix}, \quad (21)$$

for microscale periodicities $p_x = n_x = 5$ and $p_y = n_y = 4$, with patch width ratios $r_x = 0.5$ and $r_y = 0.4$. The qualitative properties of the patch simulation are like those of Figure 1 albeit here starting from a noisy initial condition. Such simulations as these are readily performed using our MATLAB/Octave Toolbox (Maclean, Bunder, and Roberts 2020).

Corollary 9 (2D self adjoint). *The 2D patch scheme (20) preserves the self-adjoint symmetry of the 2D heterogeneous diffusion (1) when the patches are coupled by spectral (Section 2.2) or Lagrangian (Section 2.3) interpolation.*

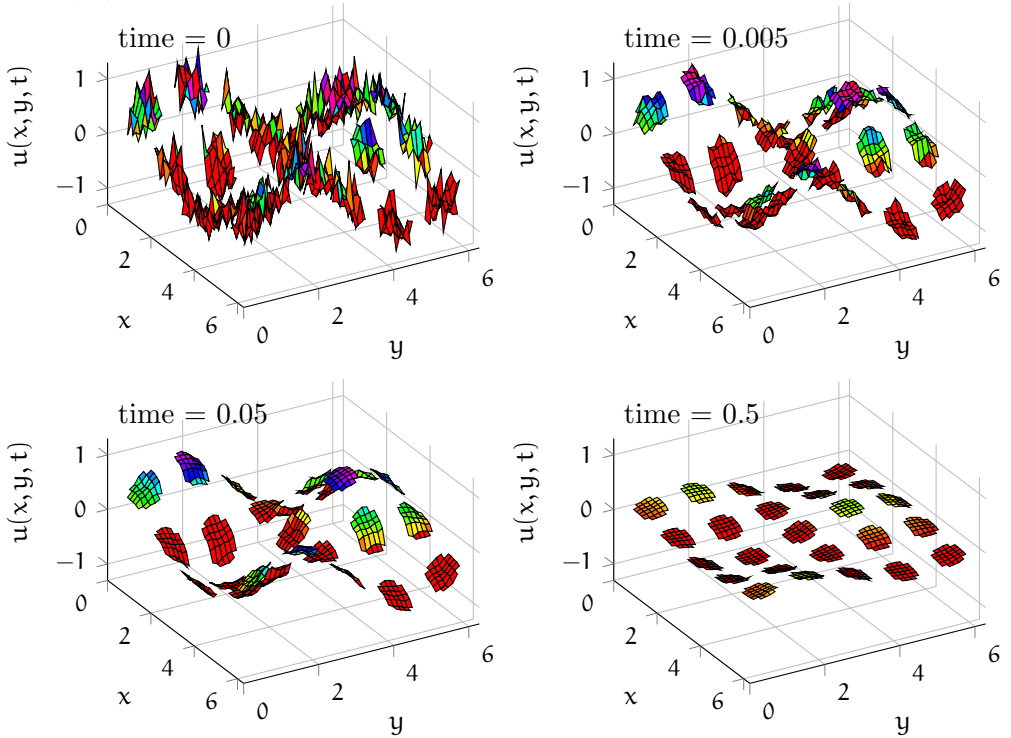
The following proof should generalise by induction to also cover corresponding patch schemes in multi-D space.

Proof. Let the space $\mathbb{H} := \mathbb{R}^{n_y N_y}$, and form all field values at fixed x , and all y , into the vectors $\mathbf{v}_i^I := (\mathbf{u}_{i,j}^{I,J}, j = 1 : n_y, J = 1 : N_y) \in \mathbb{H}$. Correspondingly form the diffusivity matrices that operate in the x -direction as $\mathcal{K}_{i\pm 1/2}^I := \text{diag}(\kappa_{i\pm 1/2,j}^I, j = 1 : n_y, J = 1 : N_y) \in \mathbb{H} \times \mathbb{H}$. Then the 2D heterogeneous diffusion (20a) becomes

$$\partial_t \mathbf{v}_i^I = [\mathcal{K}_{i+\frac{1}{2}}^I (\mathbf{v}_{i+1}^I - \mathbf{v}_i^I) + \mathcal{K}_{i-\frac{1}{2}}^I (\mathbf{v}_{i-1}^I - \mathbf{v}_i^I)] / d_x^2 + \mathcal{L}_i^I \mathbf{v}_i^I, \quad (22)$$

where $\mathcal{L}_i^I \in \mathbb{H} \times \mathbb{H}$ is the matrix of y -direction interactions and coupling (20c) at fixed x . By Lemmas 1 and 3, the \mathcal{L}_i^I are self-adjoint, and so the system-wide $\text{diag}(\mathcal{L}_i^I, i = 1 : n_x, I = 1 : N_x)$ is self-adjoint. The term $[\dots]/d_x^2$ in (22), coupled by (20b), is in a generalised form of the 1D diffusion (3),

Figure 13: Simulation of 2D heterogeneous diffusion (20) with diffusivities (21), spectral coupling, and a noisy initial condition.



and so, by Remark 2 and Lemmas 1 and 3, it also is self-adjoint. Thus (22) coupled by (20b) is self-adjoint, and hence so is the patch scheme (20). \square

Numerics verify accuracy of the scheme To verify the accuracy of the patch scheme we compare the full-space lattice dynamics of heterogeneous diffusion (1) with the two cases of the corresponding patch scheme (20), for two size ratios, $r_x, r_y = 0.5$ and 0.25 . The underlying microscale lattice system is kept the same across these three cases (the same $\mathbf{d}_x, \mathbf{d}_y$ and diffusivities). We tried dozens of cases where the microscale periodicities divide the patch sizes, and all verified that the 2D patch scheme with spectral interpolation, to computer round-off error,

- preserved the self-adjoint symmetry, and
- correctly predicted the (small magnitude) macroscale eigenvalues.

That is, the spectral patch scheme appears to be an accurate computational homogenisation (as proved subsequently by Corollary 11(b)).

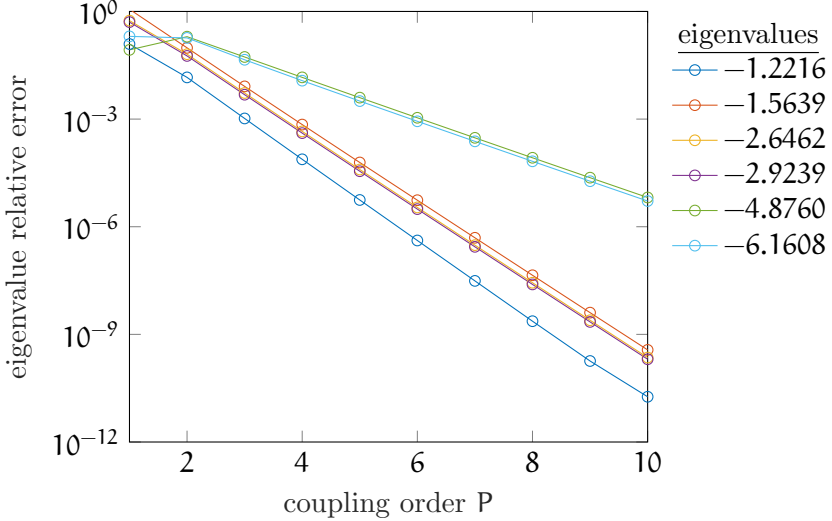
As an example of Lagrangian coupling, let's continue considering the diffusivities of (21) with the same parameters. Figure 14 plots relative errors of the macroscale eigenvalues of the 2D heterogeneous diffusion (20) for Lagrangian coupling of various orders P . The errors are relative to the accurate spectral coupling. As in the 1D case (Figure 7), Figure 14 shows the expected exponential decrease in macroscale errors as the coupling order P increases.

4.2 An ensemble of phase-shifts appears accurate

As in Section 2.4 for 1D, simulating over an ensemble of phase-shifts provides flexibility as then there are no constraints on the size of the patches. Further, Corollary 7 proves that the 1D patch scheme applied to the ensemble is consistent to arbitrarily high-order with the homogenisation of the heterogeneous diffusion. Here we discuss how to extend the 1D ensemble to the 2D case.

In 2D, the ensemble of all phase shifts of the diffusivities, such as (21), is

Figure 14: Relative errors of macroscale eigenvalues from Lagrangian coupling compared to spectral coupling for 2D heterogeneous diffusion (20) with diffusivities (21) of periodicity $p_x = 5 = n_x$, $p_y = 4 = n_y$. Other patch parameters are $N_x = 10$, $N_y = 11$, $r_x = 0.5$, $r_y = 0.4$. The right-hand column lists the eigenvalues from spectral coupling.



constructed from p_x phase-shifts in the x directions combined with p_y phase-shifts in the y direction, to give a total of $p := p_x p_y$ members in the ensemble. For computation we let $\mathbf{u}_{i,j}^{I,J}(\mathbf{t}) = (\mathbf{u}_{i,j,0}^{I,J}(\mathbf{t}), \dots, \mathbf{u}_{i,j,p-1}^{I,J}(\mathbf{t})) \in \mathbb{R}^p$ be the vector over the ensemble of field values at position (x_i^I, y_j^J) .

The ensemble microscale system within each patch is the ODEs (20a) for every member of the ensemble. For the ensemble as a whole (20a) becomes the system

$$\begin{aligned} \partial_t \mathbf{u}_{i,j}^{I,J} = & [\mathcal{K}_{i+\frac{1}{2},j}^{I,J}(\mathbf{u}_{i+1,j}^{I,J} - \mathbf{u}_{i,j}^{I,J}) + \mathcal{K}_{i-\frac{1}{2},j}^{I,J}(\mathbf{u}_{i-1,j}^{I,J} - \mathbf{u}_{i,j}^{I,J})] / d_x^2 \\ & + [\mathcal{K}_{i,j+\frac{1}{2}}^{I,J}(\mathbf{u}_{i,j+1}^{I,J} - \mathbf{u}_{i,j}^{I,J}) + \mathcal{K}_{i,j-\frac{1}{2}}^{I,J}(\mathbf{u}_{i,j-1}^{I,J} - \mathbf{u}_{i,j}^{I,J})] / d_y^2, \end{aligned} \quad (23a)$$

where diffusivity matrices $\mathcal{K}_{i,j} := \text{diag}(\kappa_{i,j}^{I,J})$, in ensemble order).

Then patches of the ensemble (23a) are coupled by a variant of (20b) and (20c). Let's introduce permutation matrices that encode the analogue of the ‘tangle’ of inter-patch communication illustrated by Figure 8. Choose the order of the ensemble in each patch so that the diffusivities $\kappa_{i,j}^{I,J}$ are independent of I, J, which can always be done as all phase-shifts are in the ensemble. Denote the ensemble vector of diffusivities, in order, on the left patch-edge to be $\boldsymbol{\kappa}_l := (\kappa_{1/2,j}) \in \mathbb{R}^p$, denote those on the right patch-edge by $\boldsymbol{\kappa}_r := (\kappa_{n_x+1/2,j}) \in \mathbb{R}^p$, and then set the permutation matrix \mathcal{P}_x such that for all $\kappa_{i,j}$ the identity $\boldsymbol{\kappa}_l = \mathcal{P}_x \boldsymbol{\kappa}_r$ holds. This permutation matrix then connects the right-edge values to the left-edge of the appropriate member of the ensemble. Similarly, set the permutation matrix \mathcal{P}_y to connect the top-edge values to the bottom-edge of the appropriate member of the ensemble. Then the inter-patch coupling conditions for the ensemble are

$$\mathbf{u}_{0,j}^{I,J} = \mathcal{P}_x \sum_K \mathcal{I}_{1n_x}^{IK} \mathbf{u}_{n_x,j}^{K,J}, \quad \mathbf{u}_{n_y+1,j}^{I,J} = \mathcal{P}_x^\dagger \sum_K \mathcal{I}_{n_x 1}^{IK} \mathbf{u}_{1,j}^{K,J}, \quad j = 1 : n_y; \quad (23b)$$

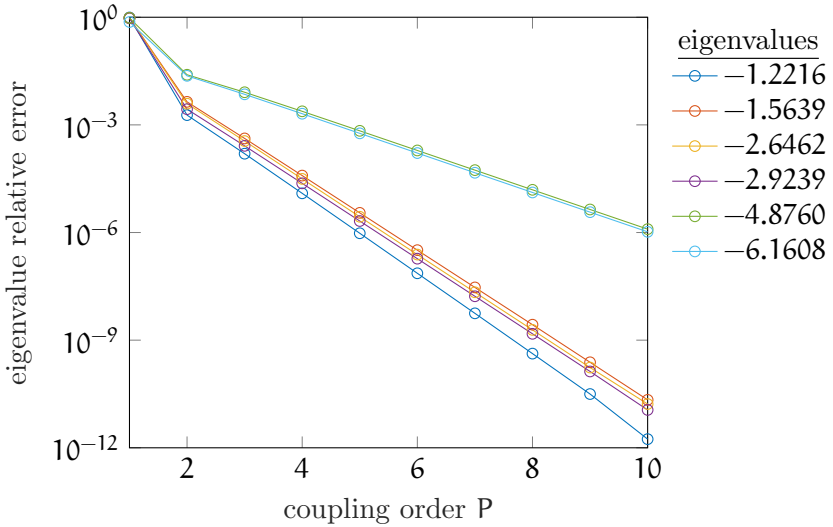
$$\mathbf{u}_{i,0}^{I,J} = \mathcal{P}_y \sum_K \mathcal{J}_{1n_y}^{JK} \mathbf{u}_{i,n_y}^{I,K}, \quad \mathbf{u}_{i,n_y+1}^{I,J} = \mathcal{P}_y^\dagger \sum_K \mathcal{J}_{n_y 1}^{JK} \mathbf{u}_{i,1}^{I,K}, \quad i = 1 : n_x, \quad (23c)$$

where coefficients \mathcal{I}_{ij}^{IJ} and \mathcal{J}_{ij}^{IJ} implement, in the x and y directions respectively, either spectral interpolation (Section 2.2) or Lagrangian interpolation (Section 2.3). Naturally generalising Corollary 9 to vector systems then asserts that this patch-ensemble system preserves the self-adjoint symmetry of the microscale heterogeneous diffusion.

Extensions to more space dimensions appear to be straightforward.

Verify accuracy in an example Consider the example of this patch-ensemble scheme (23), with Lagrangian coupling of order P , applied to the heterogeneous diffusion with diffusivities (21). The ensemble has $p = p_x p_y = 20$ members from all phase-shifts of these diffusivities. Upon numerically computing the Jacobian of this scheme, Figure 15 plots relative errors of its macroscale eigenvalues, relative to those for spectral coupling. As before, we observe the expected exponential decrease in errors with increasing order of coupling P . In order to compare with Figure 14 with its microscale spacings $d_x \approx 0.063$ and $d_y \approx 0.057$, we here decreased the width ratios,

Figure 15: Relative errors of macroscale eigenvalues from Lagrangian coupling for the 2D heterogeneous diffusion (20a), with periodicity $p_x = 5$, $p_y = 4$. We implement the ensemble of all twenty phase-shifts of the diffusivities (21). Patch parameters are $N_x = 10$, $N_y = 11$, width ratios $r_x, r_y = 0.1$, and with only $n_x = n_y = 1$. This figure and Figure 14 have the same microscale diffusion, the same d_x and d_y . The right-hand column lists the accurate eigenvalues obtained from spectral coupling.



and used the smallest possible patch sizes $n_x, n_y = 1$. Figures 14 and 15 are remarkably similar, although the ensemble here provides a smoother plot and somewhat smaller errors.

We explored many other parameter choices and observed that the ensemble always provides error plots similar to Figure 15, but that the single phase error plots were more variable, with errors in the Lagrangian coupling sometimes adversely affected by a single large diffusion coefficient.

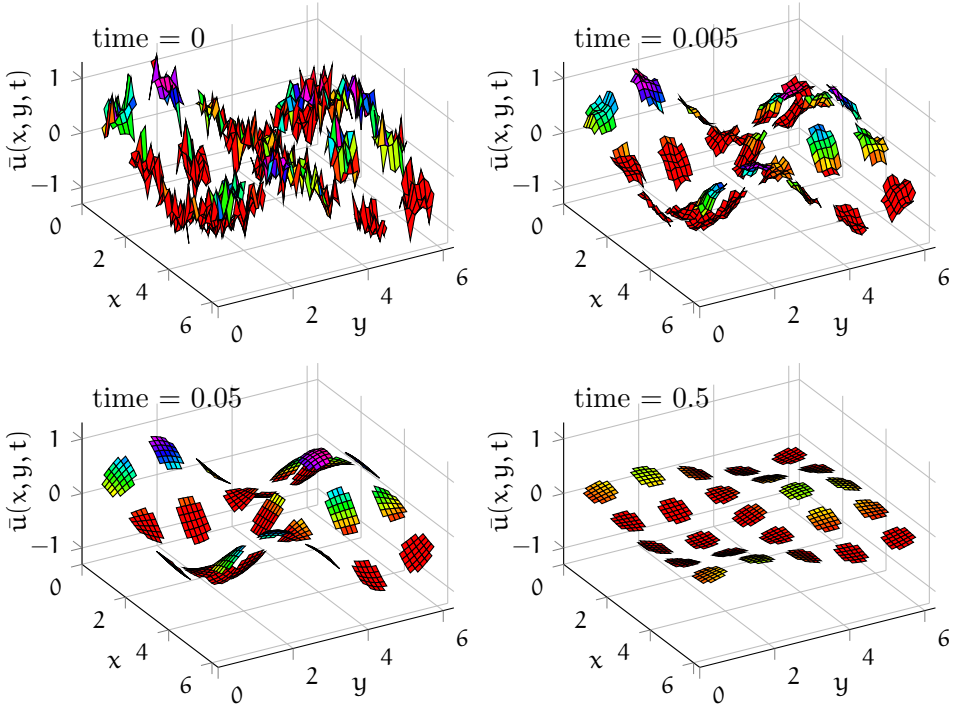
Figure 16 plots a simulation of the ensemble-mean $\bar{u}(x_i^I, y_j^J, t) := \frac{1}{p} \sum_{\ell=0}^{p-1} u_{i,j,\ell}^{I,J}(t)$ of the patch-ensemble scheme (23) for diffusivities (21)—the 2D heterogeneous diffusion (1) on patches of the twenty member ensemble of all phase-shifts of the diffusivities. It used spectral coupling via the MATLAB/Octave Toolbox (Maclean, Bunder, and Roberts 2020). For better visualisation we use only 5×5 patches, with other parameters the same as Figure 14; that is, $n_x = 5$, $n_y = 4$ and $r_x = 0.5$, $r_y = 0.4$. The initial condition is sinusoidal in x and y , plus microscale noise. The microscale noise dissipates rapidly so that by time 0.05 the simulation’s ensemble average is smooth (Figure 16). In contrast, at time 0.05 the single phase simulation (Figure 13) is ‘rough’ on the microscale, but this roughness is due to the heterogeneous diffusion rather than the initial disorder.

4.3 This 2D patch scheme is consistent to high-order

In the previous Section 4.2 our 2D patch dynamics scheme is defined in terms of an ensemble (23) with heterogeneity, defined by \mathcal{K} , varying with the spatial parameters. But for theoretical purposes the ensemble is better formed as a homogeneous system, as in Section 3 for 1D where the system (13) is homogeneous in the sense that the diffusion coefficient is independent of the spatial index.

We now form a 2D homogeneous system ensemble analogous to that of the 1D system of Figure 10. At each point (x_i, y_j) on the microscale lattice in space, there are $p = p_x p_y$ variables forming the ensemble: form them into vector $\mathbf{v}_{i,j}(t) \in \mathbb{R}^p$. Let the components of this vector be denoted $v_{i,j,k,\ell}(t)$ for $k = 0 : n_x - 1$, $\ell = 0 : n_y - 1$, and in a suitable order for the ensemble.

Figure 16: Simulation of 2D heterogeneous diffusion (20) with an ensemble of diffusion configurations constructed from (21) and spectral coupling.



Rewrite the ensemble equations in the form

$$\begin{aligned} d^2 \partial_t \mathbf{v}_{i,j,k,\ell} = & \kappa_{k+\frac{1}{2},\ell} (\mathbf{v}_{i+1,j,k+1,\ell} - \mathbf{v}_{i,j,k,\ell}) + \kappa_{k-\frac{1}{2},\ell} (\mathbf{v}_{i-1,j,k-1,\ell} - \mathbf{v}_{i,j,k,\ell}) \\ & + \kappa_{k,\ell+\frac{1}{2}} (\mathbf{v}_{i,j+1,i,\ell+1} - \mathbf{v}_{i,j,k,\ell}) + \kappa_{k,\ell-\frac{1}{2}} (\mathbf{v}_{i,j-1,i,\ell-1} - \mathbf{v}_{i,j,k,\ell}) \end{aligned} \quad (24)$$

because then the heterogeneity only varies in k, ℓ (like index ℓ in Figure 10 for the 1D case). Then $\mathbf{u}_{i,j}(\mathbf{t}) := \mathbf{v}_{i,j,i+\phi,j+\psi}$ satisfies the original heterogeneous diffusion (1), but with the diffusivities phase-shifted by ϕ, ψ , respectively. That is, the system (24) captures all the $\mathbf{p} = \mathbf{p}_x \mathbf{p}_y$ phase-shifted versions of the heterogeneous diffusion (1), but is homogeneous in the spatial indices i, j and analogous to the homogeneous 1D ensemble system (13).

Now form the vectors $\mathbf{v}_{i,j}$ from a suitable ordering of $\mathbf{v}_{i,j,k,\ell}$ so that we can write (24) in the matrix-vector form

$$\partial_t \mathbf{v}_{i,j} = \delta_i (\hat{K}_x E_i^{1/2} - \check{K}_x E_i^{-1/2}) \mathbf{v}_{i,j} + \delta_j (\hat{K}_y E_j^{1/2} - \check{K}_y E_j^{-1/2}) \mathbf{v}_{i,j} + D \mathbf{v}_{i,j}, \quad (25)$$

in terms of microscale shifts E_i and E_j , microscale centred differences δ_i and δ_j , some $\mathbf{p} \times \mathbf{p}$ cross-ensemble diffusivity matrix D , and four $\mathbf{p} \times \mathbf{p}$ off-diagonal diffusivity matrices $\hat{K}_x, \hat{K}_y, \check{K}_x$ and \check{K}_y that are *independent of location* i, j . The homogeneous matrix-vector system (25) is the 2D analogue of the 1D system (17), and is just \mathbf{p} phase-shifted copies of the original heterogeneous diffusion (1).

To proceed to analyse the patch scheme for 2D heterogeneous diffusion, we apply the patch scheme to the homogeneous (25). So, let $\mathbf{v}_{i,j}^{I,J} \in \mathbb{R}^{\mathbf{p}}$ denote the vector of field values at micro-grid point (i, j) in patch (I, J) . In the x, y -directions, respectively, let there be N_x, N_y patches, with spacing H_x, H_y , and of width h_x, h_y . Generalising (18) to 2D, apply (25) inside the patches:

$$\partial_t \mathbf{v}_{i,j}^{I,J} = \delta_i (\hat{K}_x E_i^{1/2} - \check{K}_x E_i^{-1/2}) \mathbf{v}_{i,j}^{I,J} + \delta_j (\hat{K}_y E_j^{1/2} - \check{K}_y E_j^{-1/2}) \mathbf{v}_{i,j}^{I,J} + D \mathbf{v}_{i,j}^{I,J}, \quad (26a)$$

with the inter-patch coupling that the edge-values, for every i, j, I, J ,

$$\text{(Figure 12 right)} \quad \mathbf{v}_{n+1,j}^{I,J} = E_x^{r_x} \mathbf{v}_{1,j}^{I,J}, \quad \mathbf{v}_{0,j}^{I,J} = E_x^{-r_x} \mathbf{v}_{n,j}^{I,J}, \quad (26b)$$

$$\text{(Figure 12 left)} \quad \mathbf{v}_{i,n+1}^{I,J} = E_y^{r_y} \mathbf{v}_{i,1}^{I,J}, \quad \mathbf{v}_{i,0}^{I,J} = E_y^{-r_y} \mathbf{v}_{i,n}^{I,J}. \quad (26c)$$

As in Section 3, the operators $E_x^{\pm r_x}$ and $E_y^{\pm r_y}$ are shifts across the patch widths, and may be realised and approximated by spectral or Lagrangian interpolation. Then the following generalises Theorem 6 to 2D.

Theorem 10. *The macroscale of the patch scheme (26) is consistent with the microscale dynamics of (25) over the entire spatial domain.*

As in Section 3.2, the subtlety here is that (26) holds only inside (small) patches of space, whereas (25) holds throughout space, thus forming two very different dynamical systems. The nontrivial challenge is to connect these two systems.

Proof. In essence, Theorem 10 follows because the proof of Theorem 6 applies independently to both the x and y directions.

- In the first of two steps, consider the x -direction. In this step, let the vector \mathbf{w}_i^I be the vector of values $(\mathbf{v}_{i,j}^{I,J}) \in \mathbb{R}^{p_{n_y} N_y}$ formed over $j = 1 : n_y$ and $J = 1 : N_y$. Then the system (26) takes the form

$$\partial_t \mathbf{w}_i^I = \delta_i (\hat{K}' \mathbf{w}_{i+1/2}^I - \check{K}' \mathbf{w}_{i-1/2}^I) + D' \mathbf{w}_i^I,$$

with $D' \mathbf{w}_i^I$ representing the collective over j, J of the y -direction operator $\delta_j (\hat{K}_y \mathbf{v}_{i,j+1/2}^{I,J} - \check{K}_y \mathbf{v}_{i,j-1/2}^{I,J}) + D \mathbf{v}_{i,j}^{I,J}$ coupled by (26c), and $\hat{K}' \mathbf{w}_{i+1/2}^I - \check{K}' \mathbf{w}_{i-1/2}^I$ representing the collective of $\hat{K}_x \mathbf{v}_{i+1/2,j}^{I,J} - \check{K}_x \mathbf{v}_{i-1/2,j}^{I,J}$. Further, from (26b), the \mathbf{w}_i^I -‘patches’ are coupled by

$$\mathbf{w}_{n+1}^I = E_x^{r_x} \mathbf{w}_1^I \quad \text{and} \quad \mathbf{w}_0^I = E_x^{-r_x} \mathbf{w}_n^I.$$

This \mathbf{w}_i^I -system of ‘patches’ is of the form for Theorem 6, and hence the x -direction dynamics are consistent. Specifically, upon defining the mid-‘patch’ value $\mathbf{W}^I(\mathbf{t}) := \mathbf{w}_{\bar{n}_x}^I$ for $\bar{n}_x := n_x/2 + 1/2$, from the last equation in the proof of Theorem 6 we have

$$\partial_t \mathbf{W}^I = \delta_i [(\hat{K}' E_i^{1/2} - \check{K}' E_i^{-1/2}) \mathbf{W}^I] + D' \mathbf{W}^I.$$

That is, upon unpacking the \mathbf{W}^I variables,

$$\partial_t \mathbf{v}_{\bar{n}_x,j}^{I,J} = \delta_i [(\hat{K}_x E_i^{1/2} - \check{K}_x E_i^{-1/2}) \mathbf{v}_{\bar{n}_x,j}^{I,J}]$$

$$+ \delta_j (\hat{K}_y \mathbf{v}_{\bar{n}_x, j+1/2}^{I,J} - \check{K}_y \mathbf{v}_{\bar{n}_x, j-1/2}^{I,J}) + D \mathbf{v}_{\bar{n}_x, j}^{I,J}. \quad (27)$$

- The second of the two steps is to consider the y -direction. In this step, let the vector \mathbf{w}_j^J be the vector of values $(\mathbf{v}_{\bar{n}_x, j}^{I,J}) \in \mathbb{R}^{P_{N_x}}$ formed over $I = 1 : N_x$. Then the system (27) takes the form

$$\partial_t \mathbf{w}_j^J = \delta_j (\hat{K}'' \mathbf{w}_{j+1/2}^J - \check{K}'' \mathbf{w}_{j-1/2}^J) + D'' \mathbf{w}_j^J,$$

with $D'' \mathbf{w}_j^J$ representing the collective over I of the x -direction operator $[(\hat{K}_x E_i^{1/2} - \check{K}_x E_i^{-1/2}) \mathbf{v}_{\bar{n}_x, j}^{I,J}] + D \mathbf{v}_{\bar{n}_x, j}^{I,J}$ coupled by (26b), and $\hat{K}'' \mathbf{w}_{j+1/2}^J - \check{K}'' \mathbf{w}_{j-1/2}^J$ representing the collective of $\hat{K}_y \mathbf{v}_{\bar{n}_x, j+1/2}^{I,J} - \check{K}_y \mathbf{v}_{\bar{n}_x, j-1/2}^{I,J}$. Further, from (26c), the \mathbf{w}_j^J -‘patches’ are coupled by

$$\mathbf{w}_{n+1}^J = E_y^{r_y} \mathbf{w}_1^J \quad \text{and} \quad \mathbf{w}_0^J = E_y^{-r_y} \mathbf{w}_n^J.$$

This \mathbf{w}_j^J -system of ‘patches’ is of the form for [Theorem 6](#), and hence the y -direction dynamics are consistent. Specifically, upon defining the mid-‘patch’ value $\mathbf{W}^J(t) := \mathbf{w}_{\bar{n}_y}^J = \mathbf{v}_{\bar{n}_x, \bar{n}_y}^{I,J}$ for $\bar{n}_y := n_y/2 + 1/2$, from the last equation in the proof of [Theorem 6](#) we have

$$\partial_t \mathbf{W}^J = \delta_j [(\hat{K}'' E_j^{1/2} - \check{K}'' E_j^{-1/2}) \mathbf{W}^J] + D'' \mathbf{W}^J.$$

That is, upon unpacking the \mathbf{W}^J variables, and defining the mid-patch value $\mathbf{V}^{I,J} := \mathbf{v}_{\bar{n}_x, \bar{n}_y}^{I,J}$,

$$\begin{aligned} \partial_t \mathbf{V}^{I,J} &= \delta_j [(\hat{K}_y E_j^{1/2} - \check{K}_y E_j^{-1/2}) \mathbf{V}^{I,J}] \\ &\quad + \delta_i [(\hat{K}_x E_i^{1/2} - \check{K}_x E_i^{-1/2}) \mathbf{V}^{I,J}] + D \mathbf{V}^{I,J}. \end{aligned} \quad (28)$$

The operator on the right-hand side of (28) is precisely the same as that for the microscale (25). Thus, in the patch scheme (26), the evolution over the macroscale of the mid-patch values $\mathbf{V}^{I,J}$ are consistent with the entire domain evolution of (25). \square

The following [Corollary 11](#) extends to 2D the properties of [Corollaries 7](#) and [8](#).

Corollary 11. *Consider the heterogeneous diffusion (1) with diffusivities p_x, p_y -periodic in the x, y -directions respectively.*

- 11(a) *The patch scheme applied to the ensemble (25) of the heterogeneous diffusion (1), is consistent with the homogenisation of the heterogeneous diffusion. (This consistency is illustrated by Figure 15.)*
- 11(b) *If the chosen sizes of the patches, n_x, n_y , are a multiple of the microscale periodicities, p_x, p_y , respectively, then the patch scheme applied to (1) with only one realisation of the heterogeneity (i.e., without the ensemble) has macroscale dynamics consistent with the homogenisation of the heterogeneous diffusion. (This consistency is illustrated by Figure 14.)*

Proof of Corollary 11(a). Since (25) is formed of p decoupled copies of (1), Theorem 10 implies the patch scheme (26) of (25) is thus also consistent with the original heterogeneous diffusion (1). \square

Proof of Corollary 11(b). In such scenarios each member of the ensemble (25) decouples from each other. Thus the patch scheme with only one member of the ensemble, one realisation of the phase-shift in the diffusivities, has the same macroscale dynamics as the patch scheme applied to the ensemble, and hence, by Corollary 11(a) is consistent with the heterogeneous diffusion (1). \square

5 Conclusion

This article solves a longstanding issue in equation-free macroscale modelling by providing accurate and efficient patch coupling conditions which preserve self-adjoint symmetry. By preserving symmetries we ensure that the macroscale model maintains the same conservation laws as the original microscale model. As the self-adjoint symmetry is controlled by the spatial coupling, here we have focused only on the spatial (or gap-tooth (Gear, Li, and Kevrekidis 2003)) implementation of patch dynamics, but full implementation with both patch coupling in space and projective integration in time

is straight forward with our MATLAB/Octave Toolbox (Roberts, Maclean, and Bunder 2020).

Theoretical support for our self-adjoint macroscale modelling is provided in the context of microscale heterogeneous diffusion and its homogenised dynamics on the macroscale. This is a canonical system for multiscale modelling with a rich microscale structure, and provides a basis for macroscale modelling of related but more complex systems. For other linear systems of no more than second order in space, accurate macroscale models are expected when implementing the self-adjoint patch coupling exactly as described here, as shown in the example of a heterogeneous wave (Figure 5) and also shown in the MATLAB/Octave Toolbox (Roberts, Maclean, and Bunder 2020). Further work is required for self-adjoint modelling of nonlinear problems.

For simulations, this article assumes periodic boundary conditions for the spatial domain. Adapting patch dynamics for different spatial boundary conditions is an important future task, and will build upon our current research concerning patch dynamics for shocks (Maclean et al. 2020). The multiscale modelling which accurately captures the sharp features on either side of any shock is expected to be equally effective in capturing boundary layer phenomena.

In multiscale modelling, an important consideration is how to define suitable macroscale variables which parameterise the slow manifold evolution. For the diffusion example considered here, macroscale variables are defined from averages or point samples of microscale variables, but straight forward averaging is often not possible in complex systems. For example, a microscale description of cell dynamics requires parameters to describe cell locations, velocities and interactions, but the slow macroscale dynamics might be effectively described by only time and cell distribution (Dsilva et al. 2018). Current research is designing manifold learning algorithms which apply on-the-fly simulations to determine low-dimensional parameterisations on the desired slow manifold, thus efficiently directing the simulation to the manifold of interest (Pozharskiy et al. 2020). When implemented together, patch dynamics and manifold learning should provide powerful on-the-fly computation homogenisation.

Acknowledgement This research was funded by the Australian Research Council under grants DP150102385 and DP200103097. The work of I.G.K. was also partially supported by the DARPA PAI program.

References

- Abdulle, Assyr, Doghonay Arjmand, and Edoardo Paganoni (2020). *A parabolic local problem with exponential decay of the resonance error for numerical homogenization*. Tech. rep. Institute of Mathematics, École Polytechnique Fédérale de Lausanne (cit. on p. 12).
- Abdulle, Assyr. and Marcus J. Grote (2011). “Finite Element Heterogeneous Multiscale Method for the Wave Equation”. In: *Multiscale Model. Simul.* 9.2, pp. 766–792. DOI: [10.1137/100800488](https://doi.org/10.1137/100800488) (cit. on p. 7).
- Abdulle, Assyr et al. (May 2012). “The heterogeneous multiscale method”. In: *Acta Numerica* 21, pp. 1–87. ISSN: 1474-0508. DOI: [10.1017/S0962492912000025](https://doi.org/10.1017/S0962492912000025). (Cit. on p. 12).
- Bunder, J. E., A. J. Roberts, and I. G. Kevrekidis (2017a). “Good coupling for the multiscale patch scheme on systems with microscale heterogeneity”. In: *J. Comput. Phys.* 337, pp. 154–174. DOI: [10.1016/j.jcp.2017.02.004](https://doi.org/10.1016/j.jcp.2017.02.004). (Cit. on pp. 6, 8, 11, 18, 19).
- (2017b). “Good coupling for the multiscale patch scheme on systems with microscale heterogeneity”. In: *J. Computational Physics* 337, pp. 154–174. DOI: [10.1016/j.jcp.2017.02.004](https://doi.org/10.1016/j.jcp.2017.02.004) (cit. on p. 12).
- Cao, Meng and A. J. Roberts (2015). “Multiscale modelling couples patches of non-linear wave-like simulations”. In: *IMA J. Appl. Math.* DOI: [10.1093/imamat/hxv034](https://doi.org/10.1093/imamat/hxv034). (Cit. on pp. 6, 11, 18).
- Carr, E. J., P. Perré, and I. W. Turner (2016). “The extended distributed microstructure model for gradient-driven transport: A two-scale model for bypassing effective parameters”. In: *Journal of Computational Physics* 327, pp. 810–829. DOI: [10.1016/j.jcp.2016.10.004](https://doi.org/10.1016/j.jcp.2016.10.004) (cit. on p. 8).
- Carr, J. (1981). *Applications of centre manifold theory*. Vol. 35. Applied Math. Sci. Springer–Verlag. DOI: [10.1007/978-1-4612-5929-9](https://doi.org/10.1007/978-1-4612-5929-9). (Cit. on p. 31).

- Cornaggia, Rémi and Bojan B. Guzina (Apr. 2020). “Second-order homogenization of boundary and transmission conditions for one-dimensional waves in periodic media”. In: *International Journal of Solids and Structures* 188–9, pp. 88–102. ISSN: 0020-7683. DOI: [10.1016/j.ijsolstr.2019.09.009](https://doi.org/10.1016/j.ijsolstr.2019.09.009) (cit. on pp. 8, 31).
- Dolbow, J., M. A. Khaleel, and J. Mitchell (Dec. 2004). *Multiscale Mathematics Initiative: A Roadmap. Report from the 3rd DoE Workshop on Multiscale Mathematics*. Tech. rep. Department of Energy, USA, <http://www.sc.doe.gov/ascr/mics/amr> (cit. on p. 3).
- Dsilva, Carmeline J. et al. (2018). “Parsimonious representation of nonlinear dynamical systems through manifold learning: A chemotaxis case study”. In: *Applied and Computational Harmonic Analysis* 44, pp. 759–773. DOI: [10.1016/j.acha.2015.06.008](https://doi.org/10.1016/j.acha.2015.06.008) (cit. on p. 52).
- Engquist, B. and P. E. Souganidis (2008). “Asymptotic and numerical homogenization”. In: *Acta Numerica* 17, pp. 147–190. DOI: [10.1017/S0962492906360011](https://doi.org/10.1017/S0962492906360011) (cit. on pp. 4, 7, 8).
- Engquist, Bjorn, Henrik Holst, and Olof Runborg (2011). In: *Comm. Math. Sci.* 9, pp. 33–56. DOI: [10.4310/CMS.2011.v9.n1.a2](https://doi.org/10.4310/CMS.2011.v9.n1.a2) (cit. on p. 7).
- Gear, C. W., Ju Li, and I. G. Kevrekidis (2003). “The gap-tooth method in particle simulations”. In: *Phys. Lett. A* 316, pp. 190–195. DOI: [10.1016/j.physleta.2003.07.004](https://doi.org/10.1016/j.physleta.2003.07.004) (cit. on pp. 4, 10, 51).
- Jarrad, G. A. and A. J. Roberts (2018). “Smooth subgrid fields underpin rigorous closure in spatial discretisation of reaction-advection-diffusion PDEs”. In: *Appl. Numer. Math.* 132, pp. 91–110. ISSN: 0168-9274. DOI: [10.1016/j.apnum.2018.05.011](https://doi.org/10.1016/j.apnum.2018.05.011). (Cit. on p. 6).
- Kevrekidis, I. G., C. W. Gear, and G. Hummer (2004). “Equation-free: the computer-assisted analysis of complex, multiscale systems”. In: *A. I. Ch. E. Journal* 50, pp. 1346–1354. DOI: [10.1002/aic.10106](https://doi.org/10.1002/aic.10106) (cit. on pp. 3, 4).
- Kevrekidis, Ioannis G. and Giovanni Samaey (2009). “Equation-Free Multiscale Computation: Algorithms and Applications”. In: *Annu. Rev. Phys. Chem.* 60, pp. 321–44. DOI: [10.1146/annurev.physchem.59.032607.093610](https://doi.org/10.1146/annurev.physchem.59.032607.093610) (cit. on p. 4).
- Liu, Xuan et al. (2018). *Vision 2040: A Roadmap for Integrated, Multiscale Modeling and Simulation of Materials and Systems*. NASA technical

- report, NASA/CR—2018-219771. <https://ntrs.nasa.gov/archive/nasa/casi.ntrs.nasa.gov/20180002010.pdf> (cit. on p. 3).
- Maclean, John, J. E. Bunder, and A. J. Roberts (Jan. 2020). *A toolbox of Equation-Free functions in Matlab/Octave for efficient system level simulation*. Tech. rep. <http://arxiv.org/abs/2002.01895> (cit. on pp. 6, 9, 40, 46).
- Maclean, John et al. (Mar. 2020). *A multiscale scheme accurately simulates macroscale shocks in an equation-free framework*. Tech. rep. <https://arxiv.org/abs/2002.11852> (cit. on p. 52).
- Maier, Roland and Daniel Peterseim (June 2019). “Explicit computational wave propagation in micro-heterogeneous media”. In: *BIT Numerical Mathematics* 59.2, pp. 443–462. ISSN: 1572-9125. DOI: [10.1007/s10543-018-0735-8](https://doi.org/10.1007/s10543-018-0735-8) (cit. on p. 7).
- Natl Physical Lab (1961). *Modern Computing Methods*. 2nd edition. Vol. 16. Notes on Applied Science. London: Her Majesty’s Stationery Office (cit. on p. 33).
- Owhadi, Houman (2015). “Bayesian Numerical Homogenization”. In: *Multiscale Modeling & Simulation* 13.3, pp. 812–828. DOI: [10.1137/140974596](https://doi.org/10.1137/140974596). (Cit. on p. 8).
- Peterseim, Daniel (June 2019). *Numerical Homogenization beyond Scale Separation and Periodicity*. Tech. rep. AMSI Winter School on Computational Modeling of Heterogeneous Media (cit. on p. 7).
- Pozharskiy, Dmitry et al. (Apr. 2020). *Manifold learning for accelerating coarse-grained optimization*. Tech. rep. <https://arxiv.org/abs/2001.03518> (cit. on p. 52).
- Roberts, A. J. (2010). “Choose inter-element coupling to preserve self-adjoint dynamics in multiscale modelling and computation”. In: *Appl. Numer. Math.* 60, pp. 949–973. DOI: [10.1016/j.apnum.2010.06.002](https://doi.org/10.1016/j.apnum.2010.06.002) (cit. on p. 4).
- (2015a). “Macroscale, slowly varying, models emerge from the microscale dynamics in long thin domains”. In: *IMA Journal of Applied Mathematics* 80.5, pp. 1492–1518. DOI: [10.1093/imamat/hxv004](https://doi.org/10.1093/imamat/hxv004) (cit. on pp. 30, 31).
- (2015b). *Model emergent dynamics in complex systems*. SIAM, Philadelphia. ISBN: 9781611973556. <http://bookstore.siam.org/mm20/> (cit. on pp. 30–32).

- Roberts, A. J., T. MacKenzie, and J. E. Bunder (2013). “A dynamical systems approach to simulating macroscale spatial dynamics in multiple dimensions”. In: *J. Eng. Math.* 86.1, pp. 175–207. DOI: [10.1007/s10665-013-9653-6](https://doi.org/10.1007/s10665-013-9653-6) (cit. on pp. 6, 11, 18).
- Roberts, A. J., Tony MacKenzie, and Judith Bunder (2014). “A dynamical systems approach to simulating macroscale spatial dynamics in multiple dimensions”. In: *J. Engineering Mathematics* 86.1, pp. 175–207. DOI: [10.1007/s10665-013-9653-6](https://doi.org/10.1007/s10665-013-9653-6). (Cit. on p. 35).
- Roberts, A. J., John Maclean, and J. E. Bunder (2020). *Equation-Free function toolbox for Matlab/Octave*. Tech. rep. [<https://github.com/uoal184615/EquationFreeGit>] (cit. on pp. 6, 29, 52).
- Romanazzi, Pietro, Maria Bruna, and David Howey (Aug. 2016). “Thermal homogenisation of electrical machine windings applying the multiple-scales method”. In: *Journal of Heat Transfer*. DOI: [10.1115/1.4034337](https://doi.org/10.1115/1.4034337) (cit. on p. 7).
- Runborg, Olof, Constantinos Theodoropoulos, and Ioannis G Kevrekidis (2002). “Effective bifurcation analysis: a time-stepper-based approach”. In: *Nonlinearity* 15, pp. 491–511. DOI: [10.1088/0951-7715/15/2/314](https://doi.org/10.1088/0951-7715/15/2/314) (cit. on p. 25).
- Saeb, Saba, Paul Steinmann, and Ali Javili (Sept. 2016). “Aspects of Computational Homogenization at Finite Deformations: A Unifying Review From Reuss’ to Voigt’s Bound”. In: *Applied Mechanics Reviews* 68.5. ISSN: 0003-6900. DOI: [10.1115/1.4034024](https://doi.org/10.1115/1.4034024) (cit. on pp. 4, 7, 8).
- Samaey, G., I. G. Kevrekidis, and D. Roose (2005). “The gap-tooth scheme for homogenization problems”. In: *Multiscale Modeling and Simulation* 4, pp. 278–306. DOI: [10.1137/030602046](https://doi.org/10.1137/030602046) (cit. on pp. 3, 4).
- Samaey, Giovanni, Dirk Roose, and Ioannis G. Kevrekidis (2006). “Patch dynamics with buffers for homogenization problems”. In: *J. Comput Phys.* 213, pp. 264–287. DOI: [10.1016/j.jcp.2005.08.010](https://doi.org/10.1016/j.jcp.2005.08.010) (cit. on pp. 3, 4).
- Sethna, James P. (2006). *Statistical Mechanics: Entropy, Order Parameters, and Complexity*. Oxford University Press. ISBN: 9780198566779. <http://pages.physics.cornell.edu/sethna/StatMech/> (cit. on p. 25).

- Xiu, Dongbin and Ioannis G. Kevrekidis (2005). “Equation-free, multiscale computation for unsteady random diffusion”. In: *Multiscale Model. Simul.* 4.3, pp. 915–935. DOI: [10.1137/040615006](https://doi.org/10.1137/040615006) (cit. on p. 4).
- van Kampen, N.G. (1992). *Stochastic processes in physics and chemistry*. Elsevier (cit. on p. 25).

A Macroscale homogenise of 1D diffusion

This is computer algebra script `homo1Ddiff.txt` for [Section 3.1](#).

```

1 Comment: Rigorous macroscale homogenisation of heterogeneous
2 diffusion on a lattice, p-periodic. Embed all phase shifts,
3 take Fourier transform, and construct slow manifold and
4 evolution. Time derivatives scaled by  $d^2$ . AJR, 9/4/2020;
5
6 on div; off allfac; on revpri;
7 p:=3; % microscale periodicity
8 matrix z(p+1,1),v(p+1,1),ll(p+1,p+1);
9 operator ka; % diffusivities ka(j)=kappa-{j-1/2}
10 let ka(~p)=>p; % optional example values
11 for j:=1:p do z(j,1):=1; % keep zero in p+1 element
12 % form matrix of diffusion & solvability
13 for j:=2:p do ll(j,j-1):=ll(j-1,j):=ka(j);
14 for j:=1:p-1 do ll(j,j):=-ka(j)-ka(j+1);
15 ll(p,p):=-ka(1)-ka(p)$ ll(1,p):=ll(p,1):=ll(p,1)+ka(1)$
16 for j:=1:p do ll(j,p+1):=ll(p+1,j):=-1;
17 write ll:=ll; % check print
18 ll:=1/ll$ % form inverse of diffusion & solvability
19
20 % macroscale field depends upon time
21 depend vv,t;
22 let df(vv,t)=>v(p+1,1);
23 v:=vv*z; % initial approximation
24
25 % iterate to this order of error
26 let k^5=>0;
27 expk:=for n:=0:9 sum (+i*k)^n/factorial(n);
28 exmk:=for n:=0:9 sum (-i*k)^n/factorial(n);
29 for it:=1:9 do begin
30   % compute residual
31   res:=-df(v,t); res(p+1,1):=0;
32   res(p,1):=res(p,1)+ka(1)*(expk*v(1,1)-v(p,1))$
33   res(1,1):=res(1,1)+ka(1)*(exmk*v(p,1)-v(1,1))$
34   for j:=1:p-1 do res(j,1):=res(j,1)+ka(j+1)*(expk*v(j+1,1)-v(j,1));
35   for j:=2:p do res(j,1):=res(j,1)+ka(j)*(exmk*v(j-1,1)-v(j,1));
36   % update field and evolution from residual
37   v:=v-ll*res;
38   if res=0*z then write "Success ",it:=it+10000;
39 end;
```

```
40 % write slow manifold and evolution
41 v:=v;
42 d2dvdt:=v(p+1,1);
43 end;
```